Supporting Information for

Variable Oxidation State Sulfur-Bridged Bithiazole Ligands Tune the Electronic Properties of Ruthenium(II) and Copper(I) Complexes

Elise Caron,‡ Christopher M. Brown,‡ Duane Hean and Michael O. Wolf*

Department of Chemistry, University of British Columbia, 2036 Main Mall, Vancouver, BC, Canada V6T 1Z1.

‡ These authors contributed equally to this work

TABLE of CONTENTS

NMR SPECTRA

Ruthenium(II) Complexes

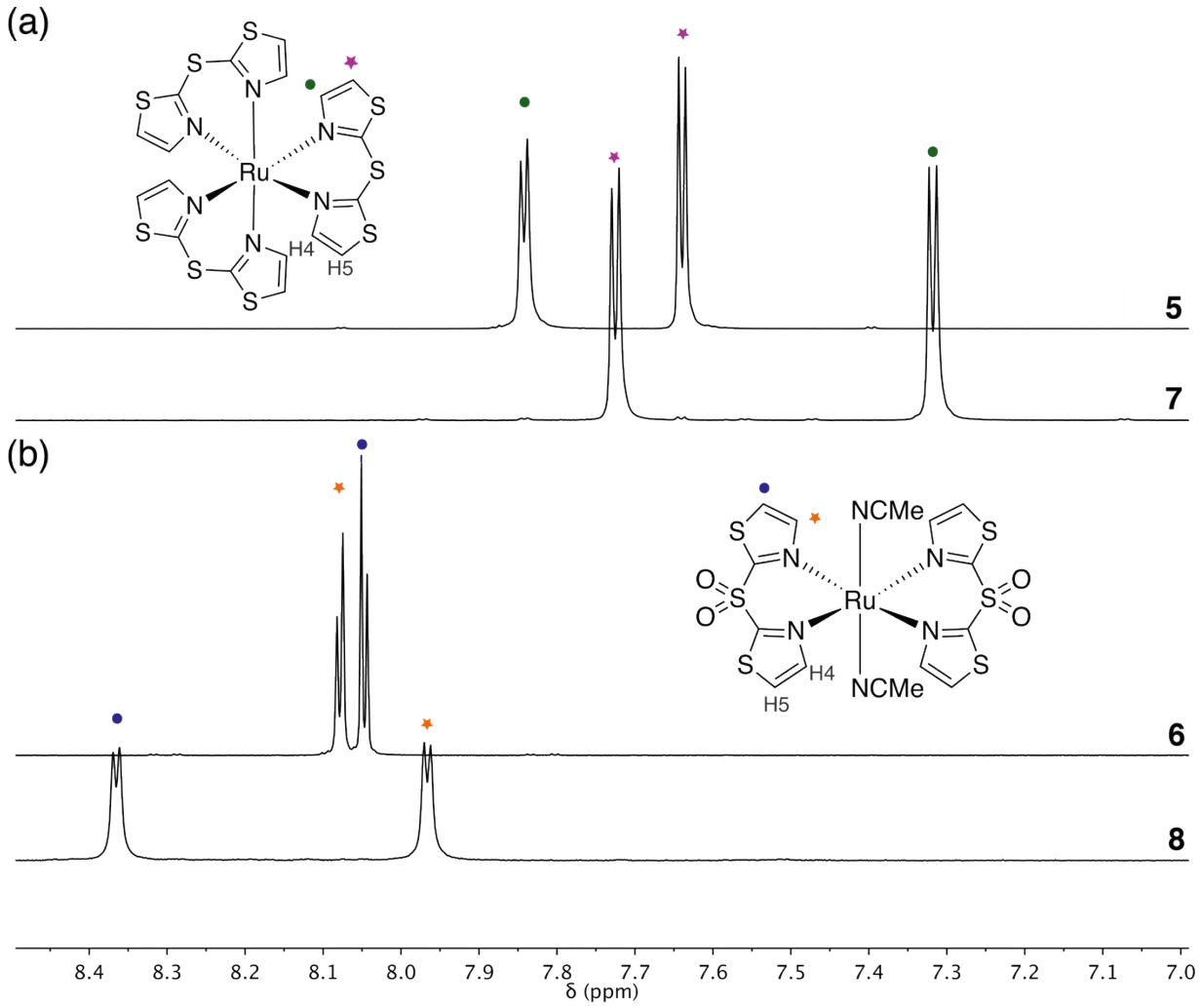

Figure S1. ^{1}H NMR spectra of pro-ligands and their respective complexes in CD_3CN at 298 K (400 MHz). (a) tzS (**5**) and $[Ru(tzS)_3][PF_6]_2$ (**7**); (b) $tzSO_2$ (**6**) and $[Ru(tzSO_2)_2(CH_3CN)_2]^{2+}$ (**8**).

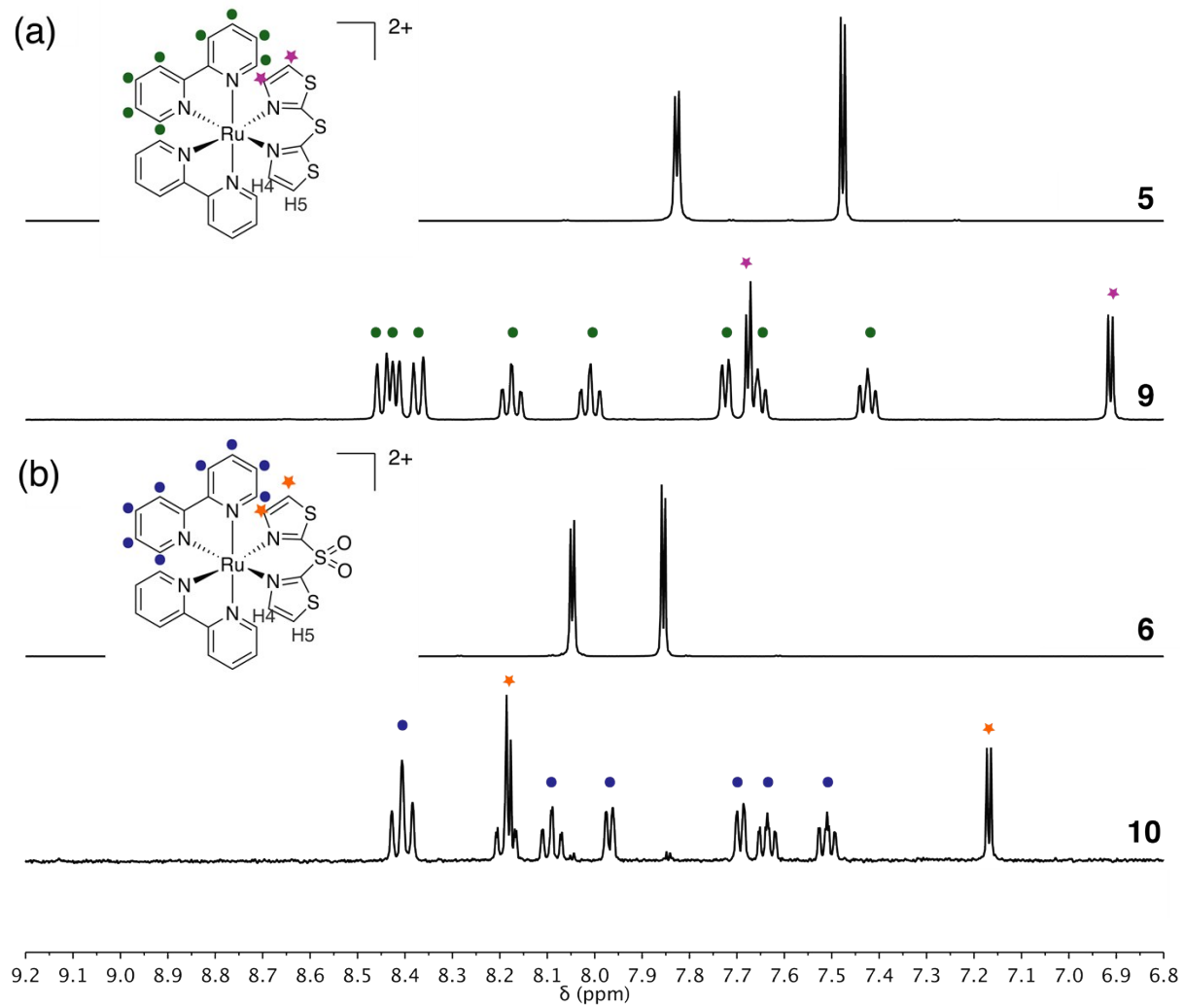

Figure S2. ^{1}H NMR spectra of pro-ligands and their respective complexes in CD_2Cl_2 at 298 K (400 MHz). (a) tzS (**5**) and $[Ru(bpy)_2(tzS)]^{2+}$ (**9**); (b) $tzSO_2$ (**6**) and $[Ru(bpy)_2(tzSO_2)]^{2+}$ (**10**).

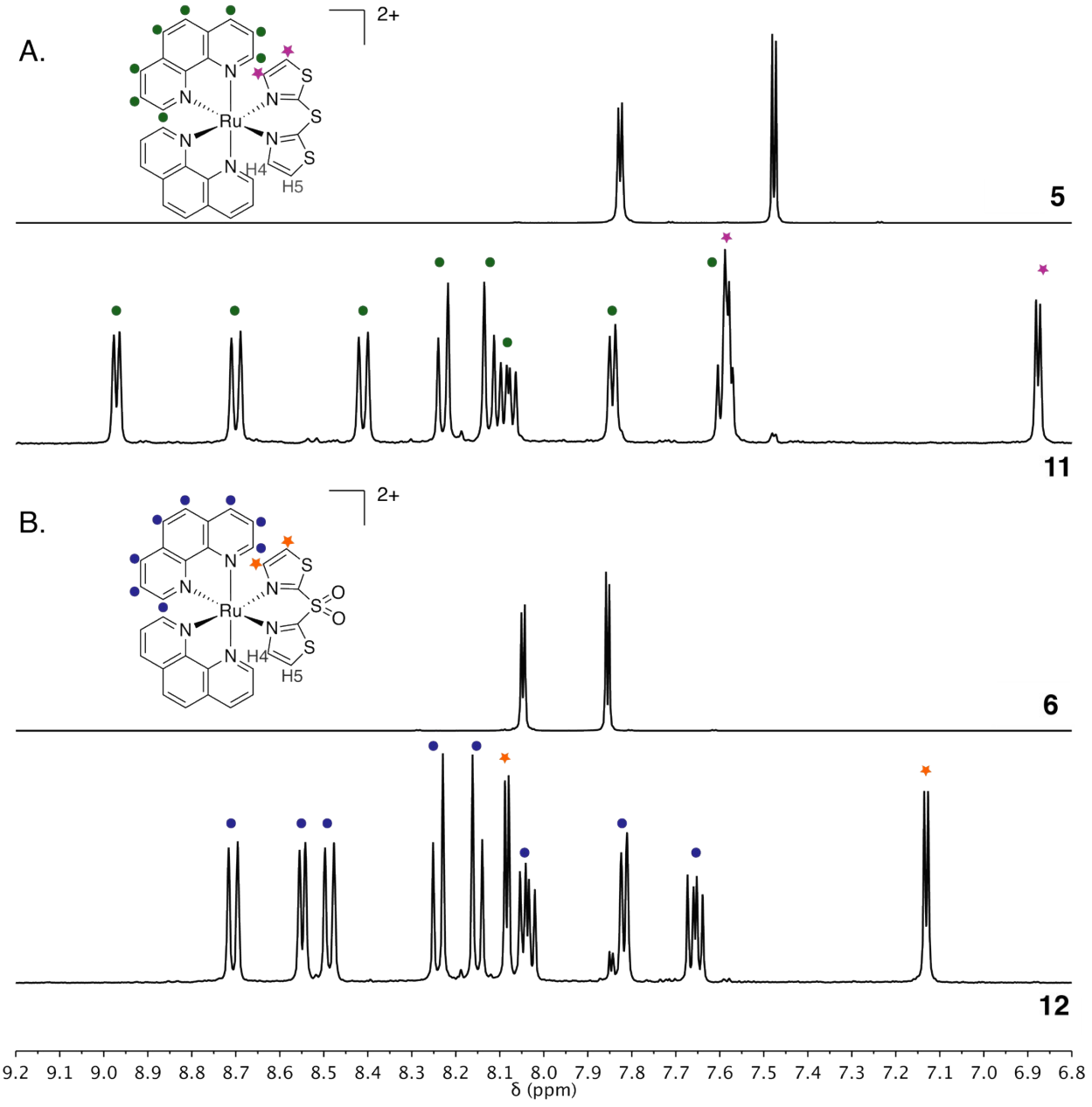

Figure S3. ^{1}H NMR spectra of pro-ligands and their respective complexes in CD_2Cl_2 at 298 K (400 MHz). (a) tzS (**5**) and $[Ru(phen)_2(tzS)]^{2+}$ (**11**); (b) $tzSO_2$ (**6**) and $[Ru(phen)_2(tzSO_2)]^{2+}$ (**12**).

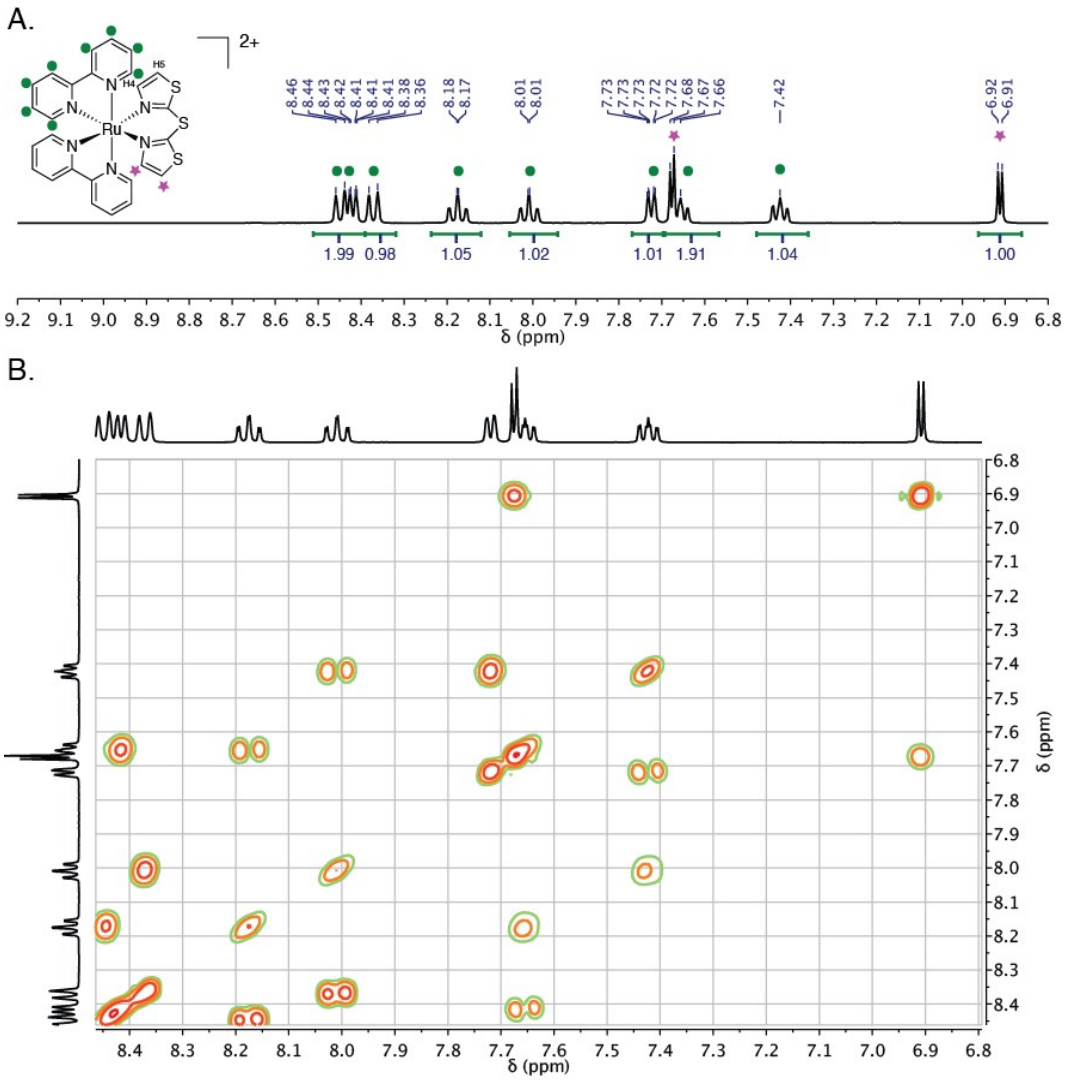

Figure S4. (a) ^{1}H and (b) COSY NMR spectra of $[Ru(bpy)_2(tzS)]^{2+}$ (**9**) in CD_2Cl_2 at 298 K (400 MHz).

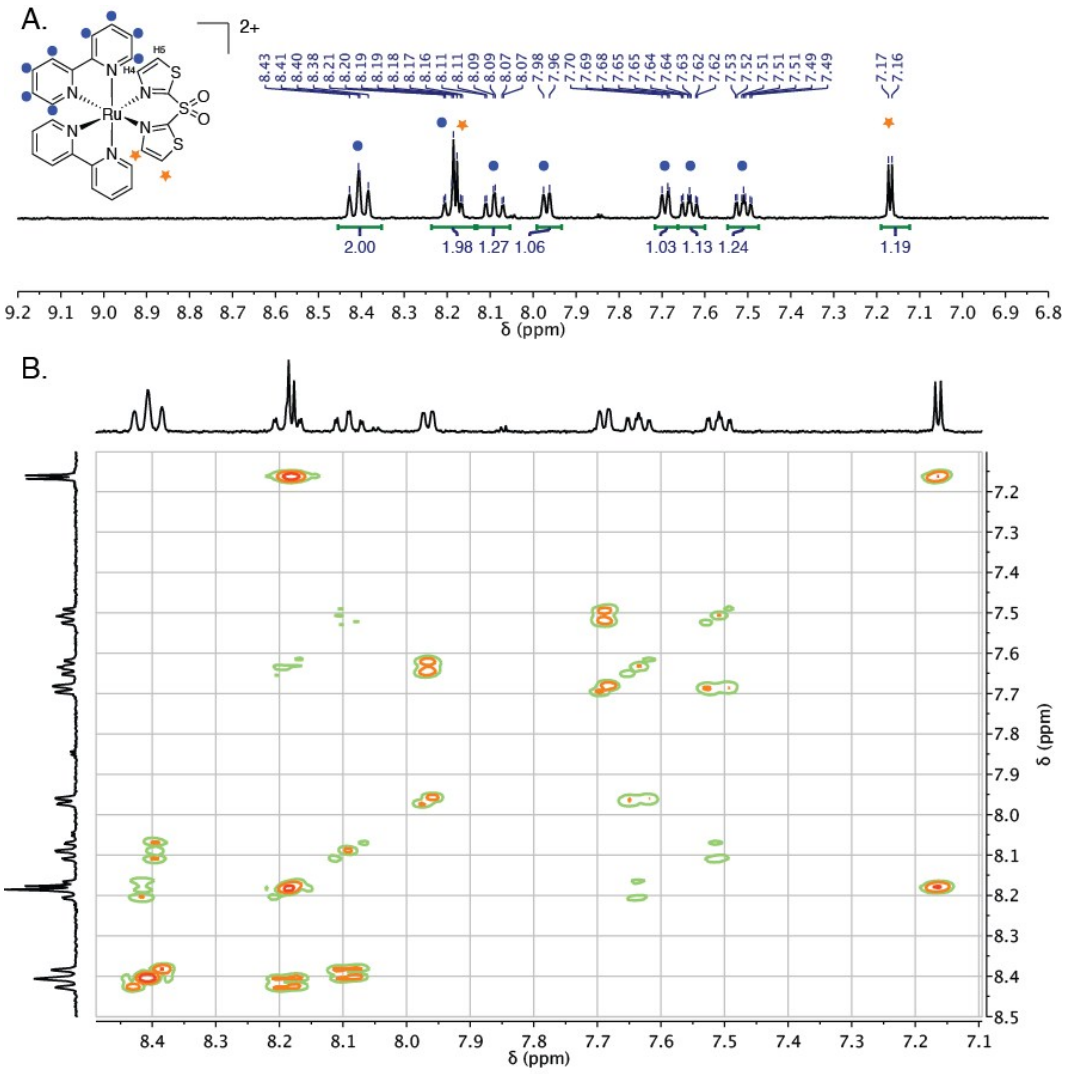

Figure S5. (a) ^{1}H and (b) COSY NMR spectra of $[Ru(bpy)_2(tzSO_2)]^{2+}$ (**10**) in CD_2Cl_2 at 298 K (400 MHz).

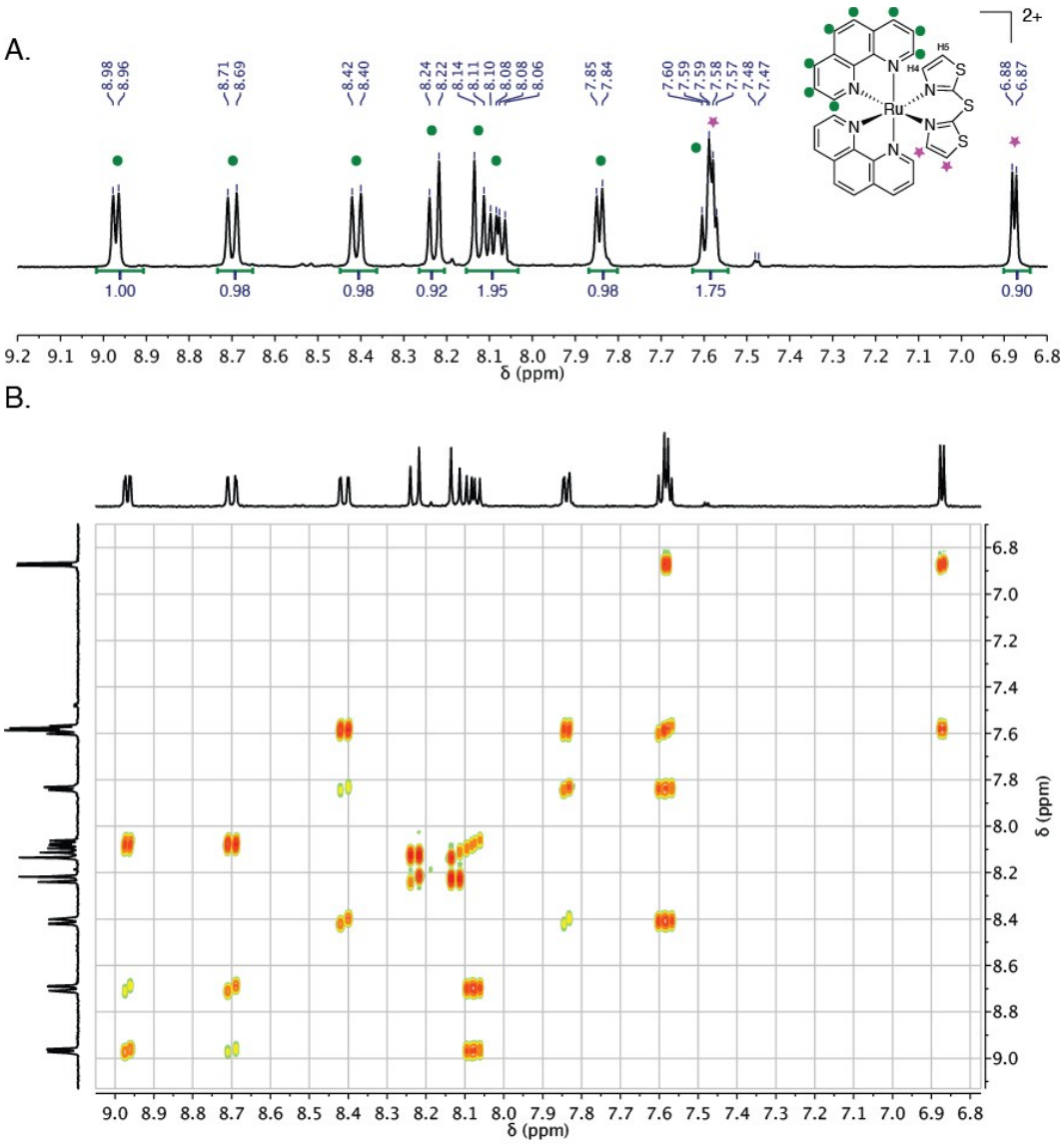

Figure S6. (a) ^{1}H and (b) COSY NMR spectra of $[Ru(phen)_2(tzS)]^{2+}$ (**11**) in CD_2Cl_2 at 298 K (400 MHz).

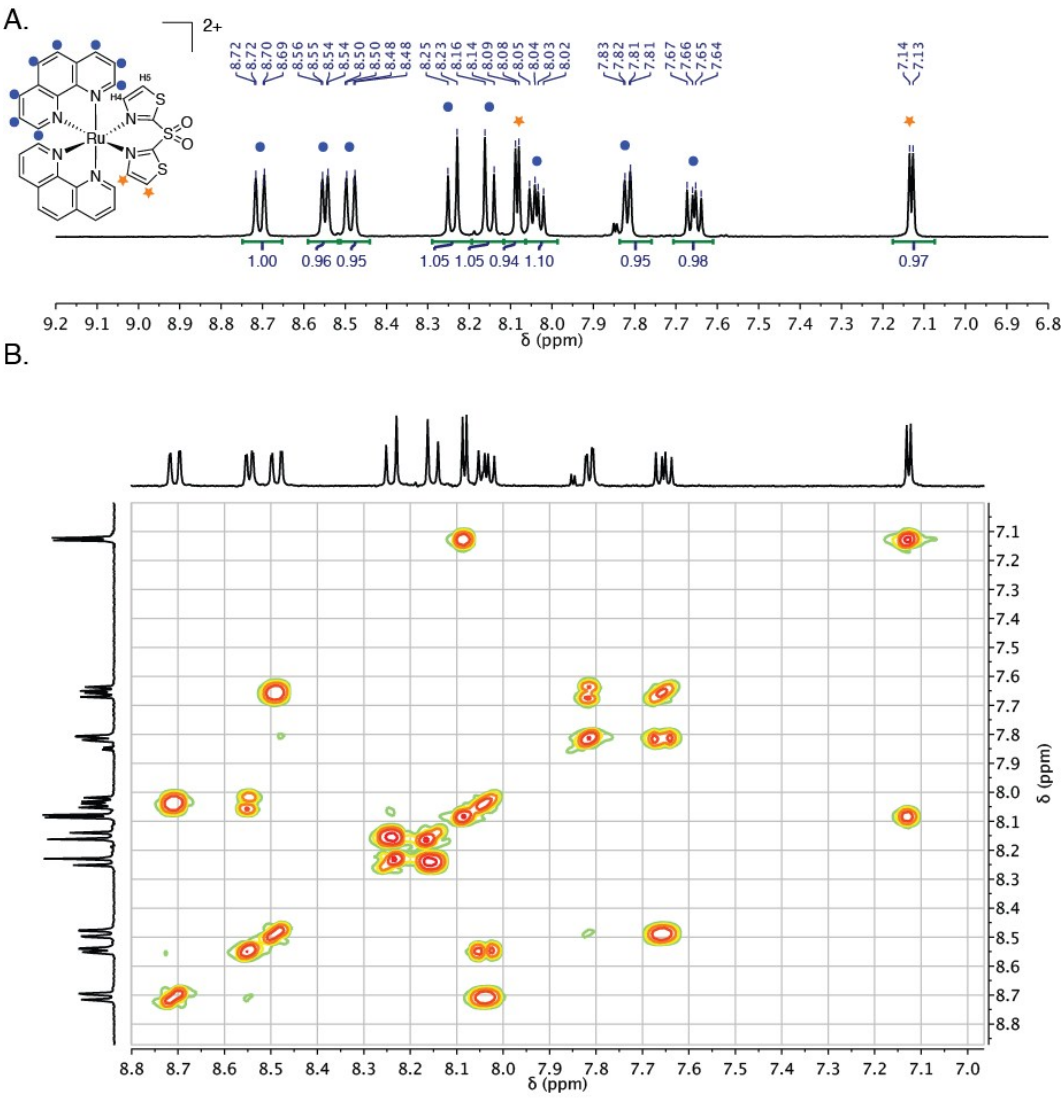

Figure S7. (a) ^{1}H and (b) COSY NMR spectra of $[Ru(phen)_2(tzSO_2)]^{2+}$ (**12**) in CD_2Cl_2 at 298 K (400 MHz).

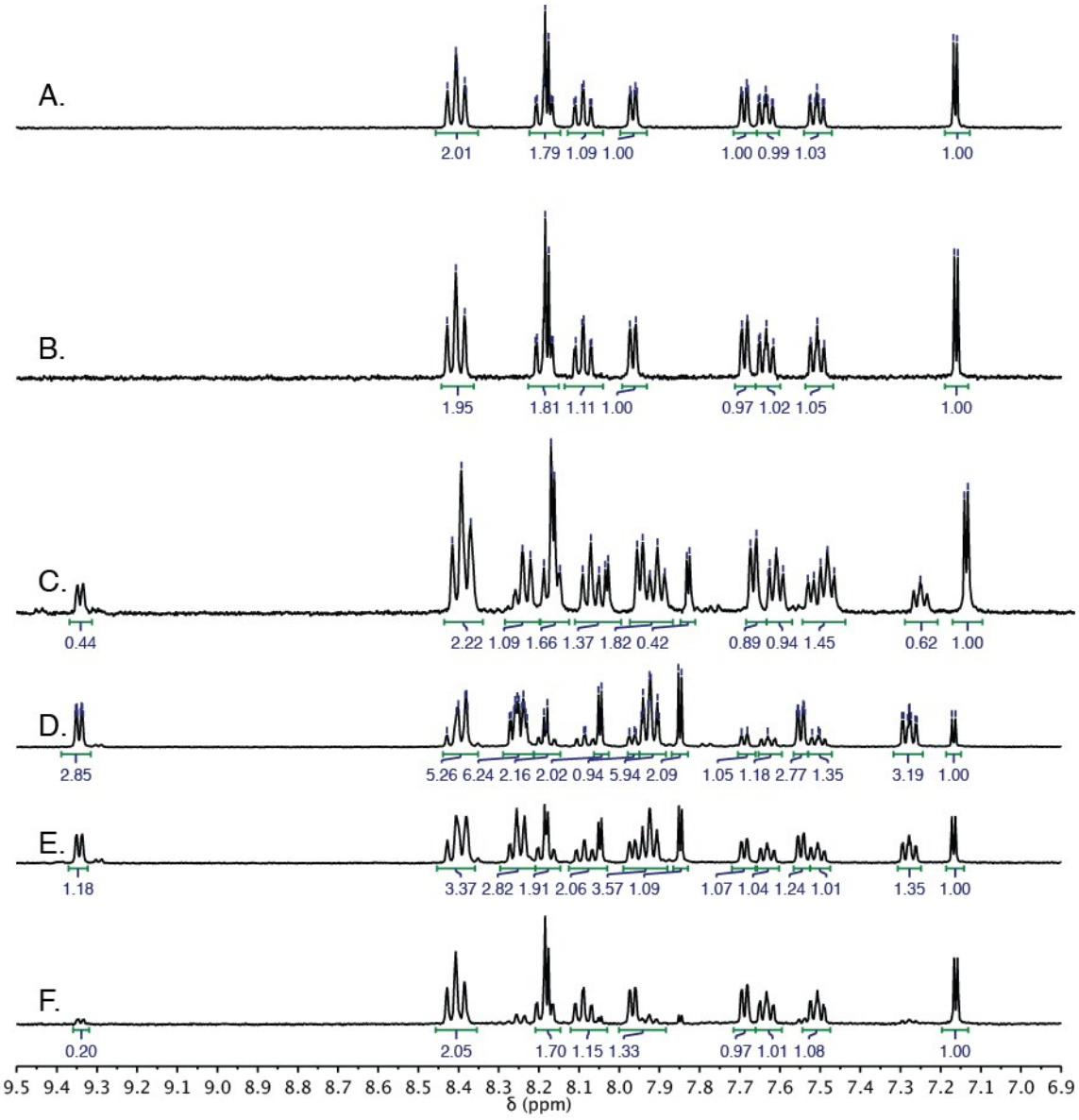

Figure S8. ^{1}H NMR photoejection experiments of $[Ru(bpy)_2(tzSO_2)]^{2+}$ (**10**) at 298 K (400 MHz). (a) CD_2Cl_2; (b) CD_2Cl_2 + 10 equiv. of CH_3CN in the dark (t = 0 min); (c) CD_2Cl_2 + 10 equiv. of CH_3CN in the dark (t = 20 min); (d) CD_2Cl_2 + 10 equiv. of CH_3CN in the sunlight (t = 2 min); (e) CD_2Cl_2 + 10 equiv. of CH_3CN under UV light (t = 15 min); (f) CD_2Cl_2 + 10 equiv. of CH_3CN under visible light (t = 15 min). *t = time after addition of CH_3CN.

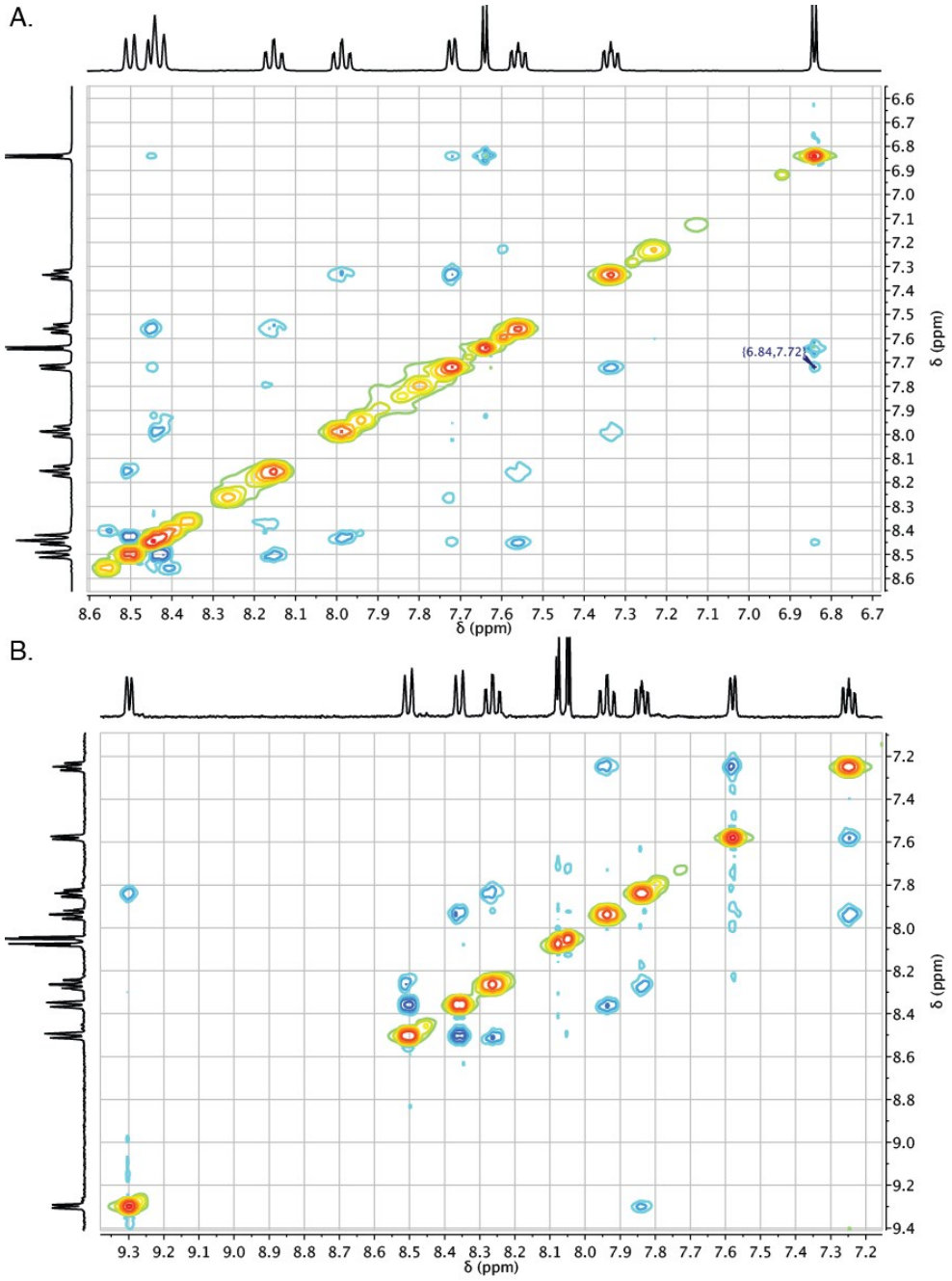

Figure S9. NOESY NMR spectra of (a) $[Ru(bpy)_2(tzS)]^{2+}$ (**9**) and (b) $[Ru(bpy)_2(tzSO_2)]^{2+}$ (**10**) in CD_3CN at 298 K (400 MHz).

Copper(I) Complexes

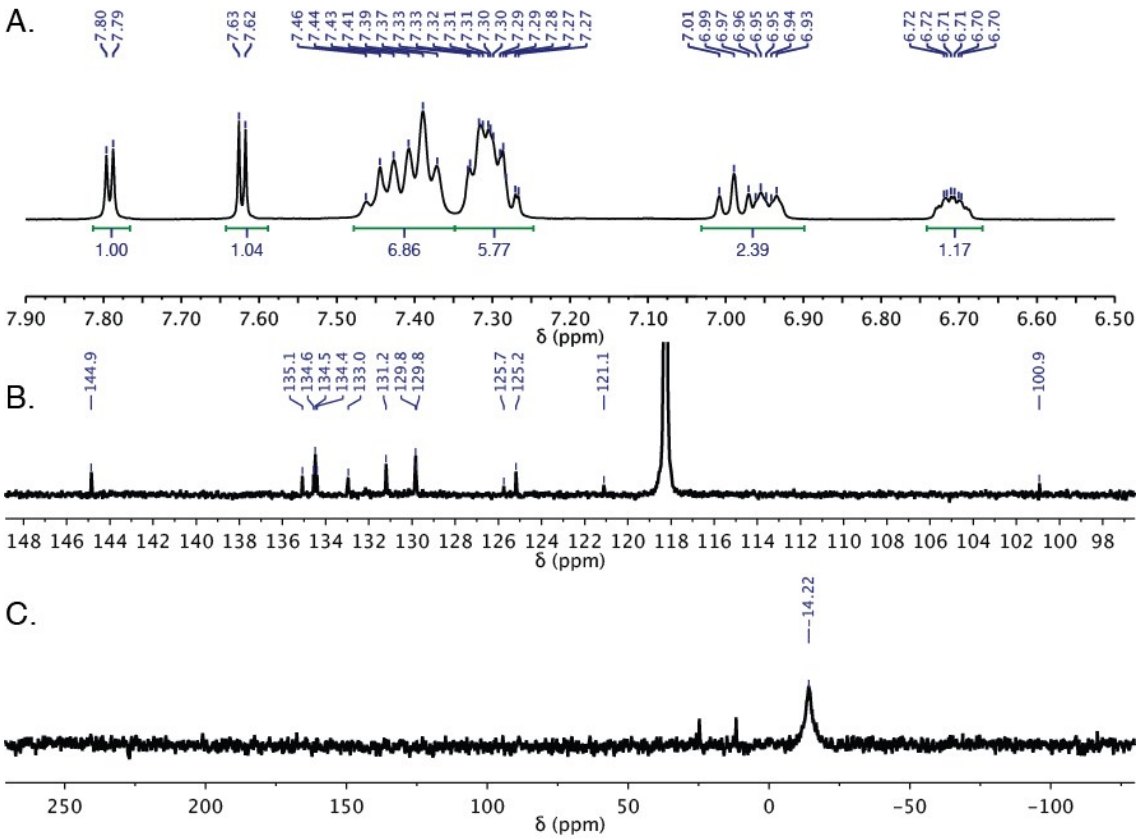

Figure S10. (a) ^{1}H; (b) $^{13}C\{^{1}H\}$; and (c) $^{31}P\{^{1}H\}$ NMR spectra of $[Cu(POP)(tzS)]^{+}$ (**13**) performed in CD_3CN at 298 K (400 MHz).

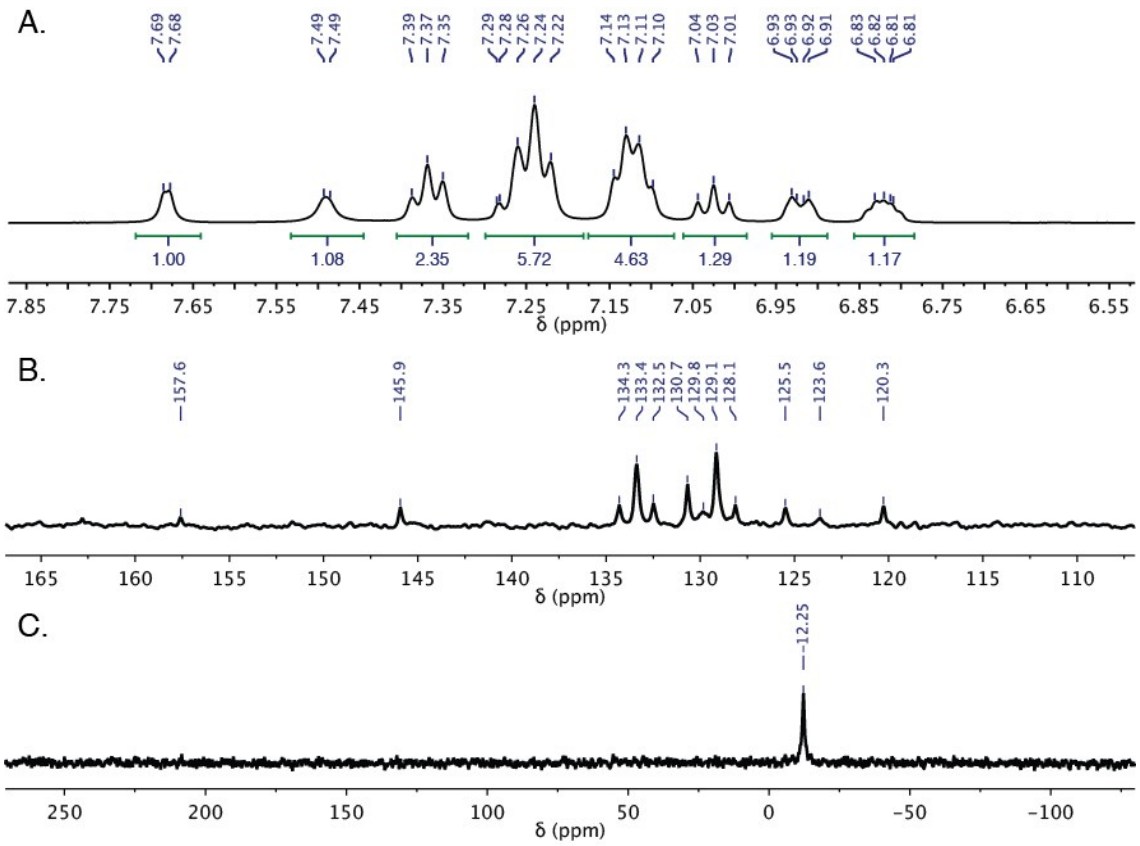

Figure S11. (a) ^{1}H; (b) $^{13}C\{^{1}H\}$; and (c) $^{31}P\{^{1}H\}$ NMR spectra of $[Cu(POP)(tzSO_2)]^+$ (**14**) in CD_2Cl_2 at 298 K (400 MHz).

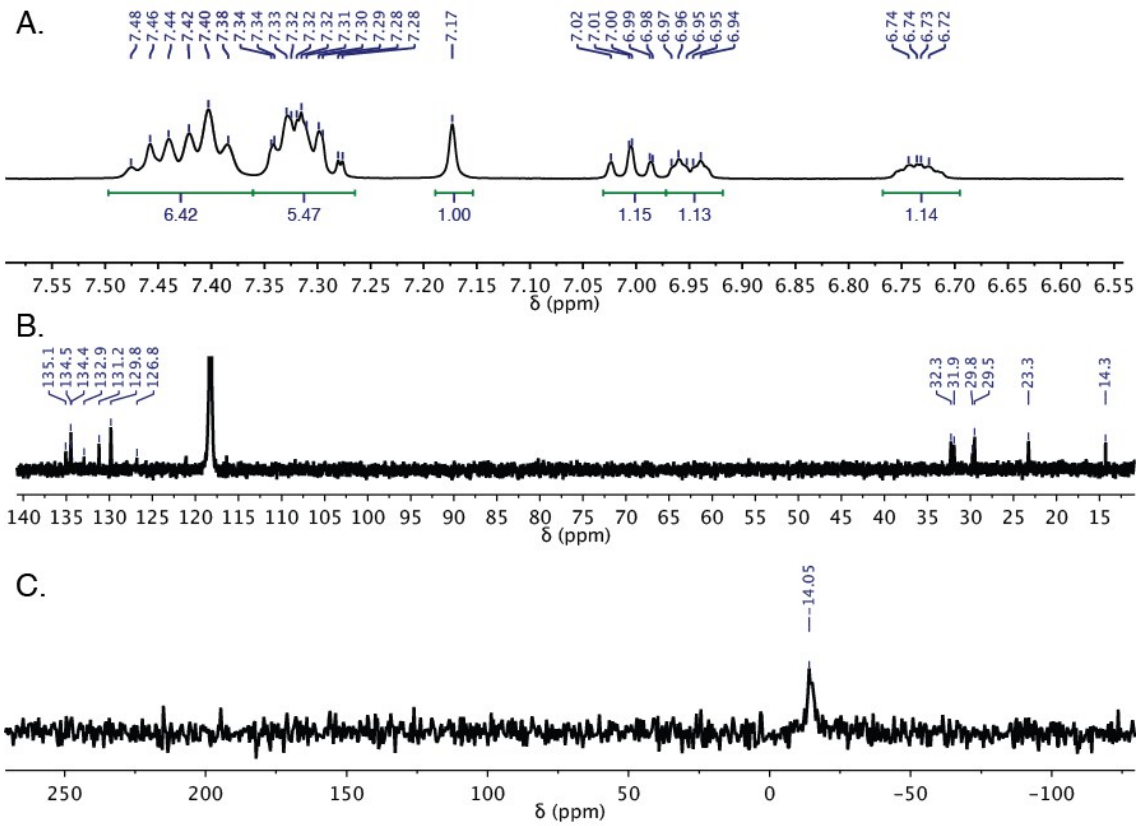

Figure S12. (a) ^{1}H; (b) $^{13}C\{^{1}H\}$; and (c) $^{31}P\{^{1}H\}$ NMR spectra of $[(POP)Cu(hbtz)Cu(POP)]^{2+}$ (**15**) in CD_3CN at 298 K (400 MHz).

X-RAY CRYSTALLOGRAPHY

Table S1. Selected crystal data and structure refinement for compounds **5**–**9**.

	tzS (**5**)	$tzSO_2$ (**6**)	$[Ru(tzS)_3][PF_6]_2$ (**7**)	$[Ru(tzSO_2)_2(MeCN)_2][PF_6]$ (**8**)	$[Ru(bpy)_2(tzS)][PF_6]_2$ (**9**)
Empirical formula	$C_6H_4N_2S_3$	$C_6H_4N_2O_2S_3$	$C_{20}H_{16}Cl_4F_{12}N_6P_2RuS_9$	$C_{16}H_{14}F_{12}N_6O_4P_2RuS_6$	$C_{26}H_{20}F_{12}N_6P_2RuS_3$
Formula weight	200.29	232.29	1161.74	937.70	903.67
Temperature/K	100(2)	100(2)	100(2)	100(2)	100(2)
Crystal system	monoclinic	monoclinic	monoclinic	orthorhombic	triclinic
Space group	Cc	$P2_1/n$	$P2_1/c$	Pbca	P-1
a/Å	5.1947(7)	5.6977(6)	20.740(2)	15.7488(10)	9.9194(10)
b/Å	13.717(2)	21.813(2)	11.2518(11)	10.2530(6)	12.2967(12)
c/Å	10.9339(16)	7.5732(11)	19.1696(19)	18.1104(11)	15.4919(16)
α/°	90	90	90	90	83.535(3)
β/°	93.100(5)	111.635(5)	110.755(5)	90	78.175(2)
γ/°	90	90	90	90	71.471(2)
Volume/$Å^3$	778.0(2)	874.93(19)	4183.1(7)	2924.3(3)	1751.4(3)
Z	4	4	4	4	2
$\rho_{calc}g/cm^3$	1.710	1.763	1.845	2.130	1.714
μ/mm^{-1}	0.878	0.810	1.237	1.191	0.811
F(000)	408.0	472.0	2288.0	1848.0	896.0
Crystal size/mm^3	0.499 × 0.401 × 0.201	0.466 × 0.301 × 0.01	0.12 × 0.117 × 0.101	0.333 × 0.304 × 0.09	0.123 × 0.101 × 0.09
Radiation	MoKα (λ = 0.71073)	MoKα (λ = 0.71073)	MoKα (λ = 0.71073)	MoKα (λ = 0.71073)	MoKα (λ = 0.71073)
2Θ range for data collection/°	5.94 to 56.66	6.082 to 56.458	4.186 to 52.926	4.498 to 56.65	3.498 to 56.64
Index ranges	-6 ≤ h ≤ 6, -18 ≤ k ≤ 17, -14 ≤ l ≤ 14	-7 ≤ h ≤ 7, -26 ≤ k ≤ 28, -10 ≤ l ≤ 10	-26 ≤ h ≤ 25, -14 ≤ k ≤ 9, -23 ≤ l ≤ 23	-21 ≤ h ≤ 16, -13 ≤ k ≤ 12, -24 ≤ l ≤ 24	-13 ≤ h ≤ 13, -16 ≤ k ≤ 16, -11 ≤ l ≤ 20

Reflections collected	6801	8655	20380	15144	30867
Independent reflections	1822 [R_{int} = 0.1098, R_{sigma} = 0.0523]	2147 [R_{int} = 0.0163, R_{sigma} = 0.0131]	8468 [R_{int} = 0.0402, R_{sigma} = 0.0648]	3639 [R_{int} = 0.0424, R_{sigma} = 0.0273]	8537 [R_{int} = 0.0240, R_{sigma} = 0.0273]
Data/restraints/parameters	1822/2/100	2147/0/118	8468/0/487	3639/0/215	8537/0/451
Goodness-of-fit on F^2	1.056	1.085	1.020	1.041	1.031
Final R indexes [I>=2σ (I)]	R_1 = 0.0344, wR_2 = 0.0878	R_1 = 0.0214, wR_2 = 0.0565	R_1 = 0.0667, wR_2 = = 0.1639	R_1 = 0.0228, wR_2 = 0.0602	R_1 = 0.0357, wR_2 = 0.0865
Final R indexes [all data]	R_1 = 0.0344, wR_2 = 0.0879	R_1 = 0.0218, wR_2 = 0.0567	R_1 = 0.0907, wR_2 = = 0.1772	R_1 = 0.0271, wR_2 = 0.0620	R_1 = 0.0443, wR_2 = 0.0910
Largest diff. peak/hole / e $Å^{-3}$	0.75/-0.46	0.42/-0.41	2.02/-1.17	0.94/-1.04	1.19/-0.77
Flack parameter	-0.08(12)				

Table S2. Selected crystal data and structure refinement for compounds **12**–**15**.

	$[Ru(phen)_2(tzSO_2)][PF_6]_2$ (**12**)	$[Cu(POP)tzS][BF_4]_2$ (**13**)	$[Cu(POP)tzSO_2][BF_4]$ (**14**)	$[Cu(POP)(hbtz)][BF_4]$ (**15**)
Empirical formula	$C_{30}H_{20}F_{12}N_6O_2P_2RuS_3$	$C_{43.49}H_{35.63}BCl_{0.34}CuF_4N_2O_{1.33}P_2S_3$	$C_{43}H_{34}BCl_2CuF_4N_2O_3P_2S_3$	$C_{98.02}H_{104.06}B_{2.04}Cu_2F_{8.16}N_2O_4P_4S_2$
Formula weight	983.71	928.05	1006.09	1866.30
Temperature/K	100(2)	100(2)	100(2)	100(2)
Crystal system	orthorhombic	monoclinic	monoclinic	triclinic
Space group	Pbca	$P2_1/n$	$P2_1/n$	P-1
a/Å	12.8317(8)	13.0385(9)	13.2844(6)	12.6003(14)
b/Å	15.2760(10)	44.590(3)	12.9331(6)	13.8878(15)
c/Å	36.552(2)	14.4382(8)	25.3545(11)	15.3231(16)
α/°	90	90	90	72.305(4)
β/°	90	94.266(2)	93.727(2)	71.948(4)
γ/°	90	90	90	66.698(4)
Volume/Å^3	7164.9(8)	8370.9(9)	4346.9(3)	2290.4(4)
Z	8	8	4	1
ρ_{calc}g/cm^3	1.824	1.473	1.537	1.353
μ/mm^{-1}	0.805	0.826	0.903	0.649
F(000)	3904.0	3800.0	2048.0	972.0
Crystal size/mm^3	0.123 × 0.101 × 0.05	0.384 × 0.111 × 0.02	0.409 × 0.208 × 0.105	0.306 × 0.257 × 0.234
Radiation	MoKα (λ = 0.71073)	MoKα (λ = 0.71073)	MoKα (λ = 0.71073)	MoKα (λ = 0.71073)
2Θ range for data collection/°	3.878 to 53.094	1.826 to 52.756	3.22 to 55.998	3.866 to 56.696
Index ranges	-16 ≤ h ≤ 16, -13 ≤ k ≤ 19, -45 ≤ l ≤ 41	-16 ≤ h ≤ 16, -47 ≤ k ≤ 55, -11 ≤ l ≤ 18	-14 ≤ h ≤ 13, -14 ≤ k ≤ 11, -25 ≤ l ≤ 28	-15 ≤ h ≤ 16, -18 ≤ k ≤ 17, -20 ≤ l ≤ 20
Reflections collected	31751	68044	30265	30305

Independent reflections	7421 [R_{int} = 0.0390, R_{sigma} = 0.0413]	17006 [R_{int} = 0.0315, R_{sigma} = 0.0320]	10029 [R_{int} = 0.0215, R_{sigma} = 0.0212]	11409 [R_{int} = 0.0201, R_{sigma} = 0.0261]
Data/restraints/parameters	7421/609/542	17006/3/1121	10029/52/560	11409/794/696
Goodness-of-fit on F^2	1.098	1.057	1.046	1.058
Final R indexes [I>=2σ (I)]	R_1 = 0.0709, wR_2 = 0.1720	R_1 = 0.0352, wR_2 = 0.0846	R_1 = 0.0278, wR_2 = 0.0701	R_1 = 0.0388, wR_2 = 0.1049
Final R indexes [all data]	R_1 = 0.0824, wR_2 = 0.1786	R_1 = 0.0442, wR_2 = 0.0886	R_1 = 0.0306, wR_2 = 0.0716	R_1 = 0.0463, wR_2 = 0.1110
Largest diff. peak/hole / e $Å^{-3}$	3.53/-1.23	0.66/-0.73	0.66/-0.50	0.62/-0.72

Table S3. Selected bond angles for pro-ligands tzS (**5**) and tzSO2 (**6**).

tzS (**5**)	Bond angle (º)	$tzSO_2$ (**6**)	Bond angle (º)
C1-S1-C4	101.66(14)	C1-S1-C4	104.62(5)

Table S4. Selected bond lengths for compounds $[Ru(tzS)_3][PF_6]_2$ (**7**), $[Ru(tzSO_2)_2(MeCN)_2][PF_6]$ (**8**), $[Ru(bpy)_2(tzS)][PF_6]_2$ (**9**) and $[Ru(phen)_2(tzSO_2)][PF_6]_2$ (**12**).

$[Ru(tzS)_3][PF_6]_2$ (**7**)	Length (Å)	$[Ru(tzSO_2)_2(MeCN)_2][PF_6]$ (**8**)	Length (Å)
Ru1-N1	2.087(5)	Ru1-N1	2.0766(14)
Ru1-N2	2.092(5)	Ru1-N1[1]	2.0766(14)
Ru1-N3	2.078(5)	Ru1-N2	2.0811(14)
Ru1-N4	2.088(5)	Ru1-N2[1]	2.0811(14)
Ru1-N5	2.099(5)	Ru1-N3	2.0206(14)
Ru1-N6	2.127(5)	Ru1-N3[1]	2.0206(14)
S1-C3	1.754(6)	S1-C3	1.7575(17)
S1-C4	1.747(7)	S1-C4	1.7621(17)
S4-C9	1.756(7)		
S4-C10	1.748(8)		
S4-C9	1.756(7)		
S7-C15	1.755(7)		
S7-C16	1.750(7)		
$[Ru(bpy)_2(tzS)][PF_6]_2$ (**9**)	Length (Å)	$[Ru(phen)_2(tzSO_2)][PF_6]_2$ (**12**)	Length (Å)
Ru1-N1	2.085(2)	Ru1-N1	2.104(5)
Ru1-N2	2.094(2)	Ru1-N2	2.105(5)
Ru1-N3	2.070(2)	Ru1-N3	2.053(5)
Ru1-N4	2.049(2)	Ru1-N4	2.082(5)
Ru1-N5	2.057(2)	Ru1-N5	2.064(5)
Ru1-N6	2.074(2)	Ru1-N6	2.070(5)
S1-C3	1.758(3)	S1-C3	1.765(6)
S1-C4	1.759(3)	S1-C4	1.753(6)

Table S5. Selected bond angles for compounds $[Ru(tzS)_3][PF_6]_2$ (**7**), $[Ru(tzSO_2)_2(MeCN)_2][PF_6]$ (**8**), $[Ru(bpy)_2(tzS)][PF_6]_2$ (**9**) and $[Ru(phen)_2(tzSO_2)][PF_6]_2$ (**12**).

$[Ru(tzS)_3][PF_6]_2$ (**7**)	Angle (˚)	$[Ru(tzSO_2)_2(MeCN)_2][PF_6]$ (**8**)	Angle (˚)
N1-Ru1-N4	89.30(19)	N1-Ru1-N2	87.56(5)
N1-Ru1-N2	90.6(2)	N1-Ru1-N2^1	92.44(5)
N1-Ru1-N5	94.0(2)	N1^1-Ru1-N2^1	87.56(5)
N1-Ru1-N6	88.4(2)	N1^1-Ru1-N2	92.44(5)
N2-Ru1-N5	175.1(2)	N3^1-Ru1-N2^1	86.41(5)
N2-Ru1-N6	90.5(2)	N3^1-Ru1-N2	93.59(5)
N3-Ru1-N4	89.85(19)	N3-Ru1-N2	86.41(5)
N3-Ru1-N2	91.4(2)	N3-Ru1-N2^1	93.59(5)
N3-Ru1-N5	84.0(2)	N3^1-Ru1-N1	90.91(5)
N3-Ru1-N1	177.8(2)	N3-Ru1-N1	89.09(5)
N3-Ru1-N6	92.5(2)	N3-Ru1-N1^1	90.91(5)
N5-Ru1-N6	91.6(2)	N3^1-Ru1-N1^1	89.09(5)
C4-S1-C3	101.2(3)	C3-S1-C4	102.05(8)
C10-S4-C9	99.9(3)		
C16-S7-C15	105.1(3)		
$[Ru(bpy)_2(tzS)][PF_6]_2$ (**9**)	Angle (˚)	$[Ru(phen)_2(tzSO_2)][PF_6]_2$ (**12**)	Angle (˚)
N1-Ru1-N2	88.41(8)	N1-Ru1-N2	90.75(18)
N3-Ru1-N1	93.31(9)	N3-Ru1-N6	91.47(19)
N3-Ru1-N2	85.03(8)	N3-Ru1-N5	90.08(19)
N4-Ru1-N2	93.68(8)	N3-Ru1-N2	88.60(18)
N4-Ru1-N3	79.64(9)	N3-Ru1-N4	79.71(19)
N4-Ru1-N5	88.22(8)	N4-Ru1-N1	99.93(19)
N4-Ru1-N6	94.84(8)	N4-Ru1-N2	90.11(18)
N5-Ru1-N1	90.16(8)	N5-Ru1-N1	90.61(19)
N5-Ru1-N3	98.77(8)	N5-Ru1-N6	80.13(19)
N5-Ru1-N6	78.78(8)	N5-Ru1-N4	95.29(19)

N6-Ru1-N1	92.09(8)	N6-Ru1-N1	88.94(18)
N6-Ru1-N2	97.55(8)	N6-Ru1-N2	94.18(18)
C3-S1-C4	99.15(12)	C4-S1-C3	103.3(3)

Table S6. Selected bond lengths for compounds $[Cu(POP)tzS][BF_4]_2$ (**13**), $[Cu(POP)tzSO_2][BF_4]$ (**14**) and $[Cu(POP)(hbtz)][BF_4]$ (**15**).

$[Cu(POP)tzS][BF_4]_2$ (**13**)	Length (Å)	$[Cu(POP)tzSO_2][BF_4]$ (**14**)	Length (Å)
Cu1A-P1A	2.2555(6)	Cu1-N1	2.1229(18)
Cu1A-P2A	2.2418(6)	Cu1-N2	2.0867(18)
Cu1A-N1A	2.0489(18)	S1-O2	1.4297(16)
Cu1A-N2A	2.0548(18)	S1-O3	1.4367(16)
Cu1B-P1B	2.2531(6)	Cu1-P1	2.2352(6)
Cu1B-P2B	2.2827(6)	Cu1-P2	2.2741(6)
Cu1B-N1B	2.1007(17)	S1-C3	1.762(4)
Cu1B-N2B	2.0810(18)	S1-C4	1.761(4)
S1A-C3A	1.757(2)		
S1A-C4A	1.753(3)		
S1B-C3B	1.765(2)		
S1B-C4B	1.763(2)		

$[Cu(POP)(hbtz)][BF_4]$ (**15**)	Length (Å)
Cu1-N1	1.9764(16)
Cu1-P1	2.2343(5)
Cu1-P2	2.2247(5)

Table S7. Selected bond angles for compounds [Cu(POP)tzS][BF_4]$_2$ (**13**), [Cu(POP)tzSO_2][BF_4] (**14**) and [Cu(POP)(hbtz)][BF_4] (**15**).

[Cu(POP)tzS][BF_4]$_2$ (**13**)	Angle (˚)	[Cu(POP)tzSO_2][BF_4] (**14**)	Angle (˚)
P2A-Cu1A-P1A	114.43(2)	N1-Cu1-P1	127.88(9)
N1A-Cu1A-P1A	111.54(5)	N1-Cu1-P2	102.00(9)
N1A-Cu1A-P2A	111.47(5)	N2-Cu1-N1	93.50(12)
N1A-Cu1A-N2A	93.40(7)	N2-Cu1-P1	110.60(9)
N2A-Cu1A-P1A	112.70(5)	N2-Cu1-P2	108.60(9)
N2A-Cu1A-P2A	111.49(5)	P1-Cu1-P2	111.97(4)
C4A-S1A-C3A	102.98(11)	C4-S1-C3	101.17(18)
P1B-Cu1B-P2B	111.74(2)		
N1B-Cu1B-P1B	112.69(5)		
N1B-Cu1B-P2B	107.01(5)		
N2B-Cu1B-P1B	121.96(5)		
N2B-Cu1B-P2B	109.87(5)		
N2B-Cu1B-N1B	91.13(7)		
C4B-S1B-C3B	98.69(10)		
[Cu(POP)(hbtz)][BF_4] (**15**)	Angle (˚)		
P2-Cu1-P1	119.924(19)		
N1-Cu1-P1	118.33(5)		
N1-Cu1-P2	119.10(5)		

CRYSTALLOGRAPHIC DETAILS AND ORTEP DIAGRAMS

Pro-Ligands

tzS (**5**)

A colorless rectangular crystal of $C_6H_4N_2S_3$, having approximate dimensions of 0.50 × 0.40 × 0.20 mm was mounted on a nylon loop. The data were collected at a temperature of -183.0 + 0.1°C to a maximum 2Θ value of 56.6°. Data were collected in a series of ϕ and ω scans in 0.5° oscillations using 10.0-second exposures. Of the 6801 reflections that were collected, 1822 were unique (Rint = 0.11); equivalent reflections were merged. All non-hydrogen atoms were refined anisotropically. All hydrogen atoms were placed in calculated positions. The final cycle of full-matrix least-squares refinement on F^2 was based on 6801 reflections and 100 variable parameters and converged. All refinements were performed using the ShelXL[6] via the OLEX2[7] interface.

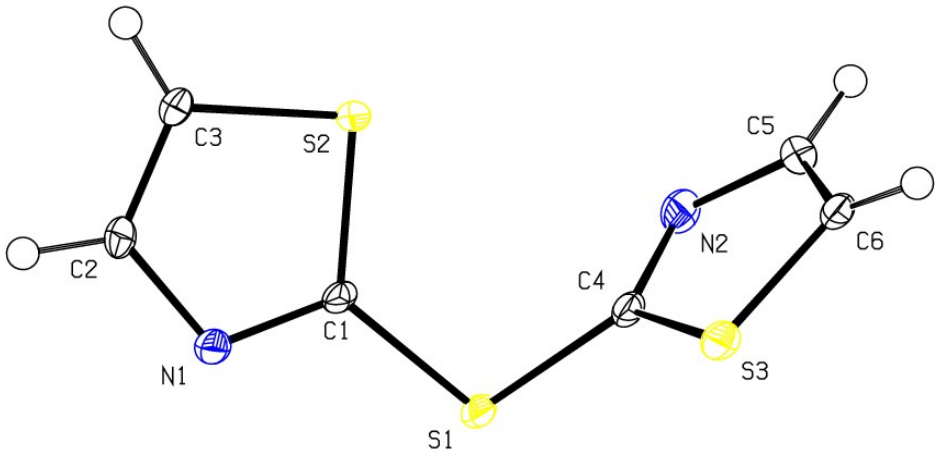

Figure S13. Asymmetric unit of **5** with thermal ellipsoids drawn are at 50 % probability level.

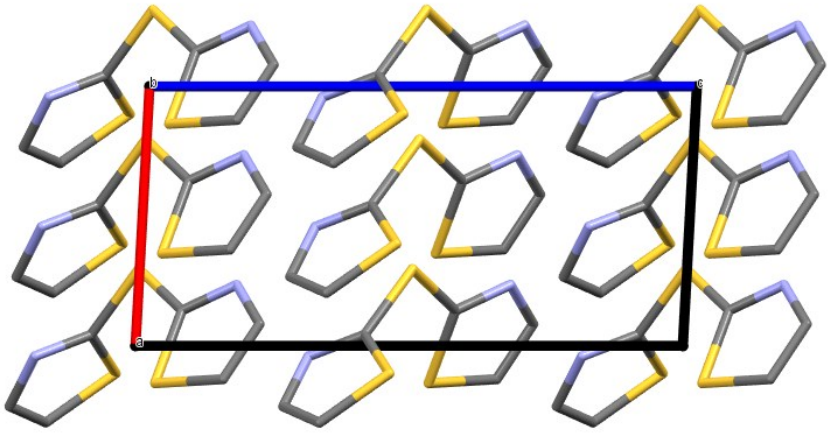

Figure S14. Packing diagram of **5** viewed along the b-axis. Hydrogen atoms are excluded for clarity.

$tzSO_2$ (**6**)

A colorless rectangular crystal of $C_6H_4N_2O_2S_3$, having approximate dimensions of 0.47 × 0.30 × 0.01 mm was mounted on a nylon loop. The data were collected at a temperature of -183.0 + 0.1°C to a maximum 2Θ value of 56.5°. Data were collected in a series of ϕ and ω scans in 0.5° oscillations using 10.0-second exposures. Of the 8655 reflections that were collected, 2147 were unique (Rint = 0.016); equivalent reflections were merged. All non-hydrogen atoms were refined anisotropically. All hydrogen atoms were placed in calculated positions. The final cycle of full-matrix least-squares refinement on F^2 was based on 8655 reflections and 118 variable parameters and converged. All refinements were performed using the ShelXL[1] via the OLEX2[2] interface. ORTEP diagrams were generated using PLATON[3].

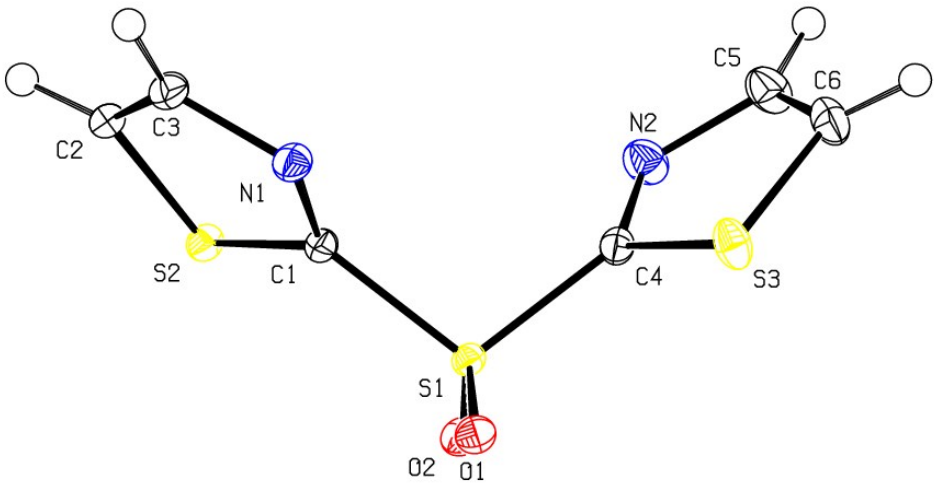

Figure S15. Asymmetric unit of **6** with thermal ellipsoids drawn are at 50 % probability level.

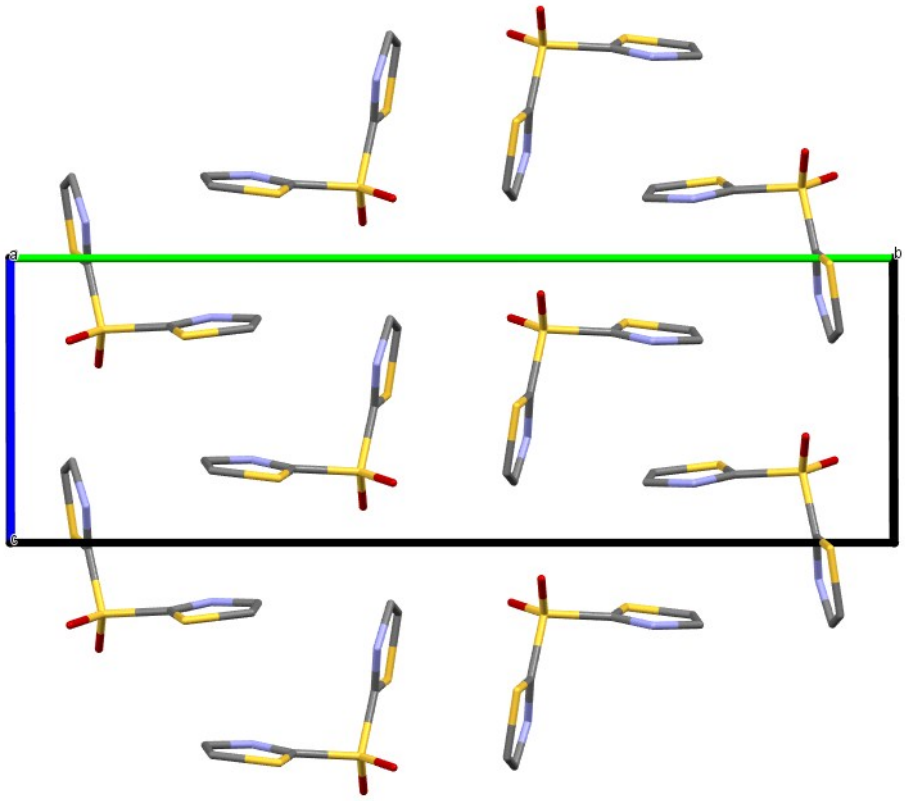

Figure S16. Packing diagram of **6** viewed along the a-axis. Hydrogen atoms are excluded for clarity.

Ruthenium(II) Complexes

$[Ru(tzS)_3][PF_6]_2$ (**7**)

A yellow plate shaped crystal of $C_{18}H_{12}F_{12}N_6P_2RuS_9 \cdot 2CH_2Cl_2$, having approximate dimensions of 0.12 × 0.12 × 0.10 mm was mounted on a nylon loop. The data were collected at a temperature of -183.0 + 0.1°C to a maximum 2Θ value of 52.9°. Data were collected in a series of ϕ and ω scans in 0.5° oscillations using 10.0-second exposures. Of the 20380 reflections that were collected, 8468 were unique (Rint = 0.040); equivalent reflections were merged. The material crystallized with two molecules of CH_2Cl_2 in the asymmetric unit. All non-hydrogen atoms were refined anisotropically. All hydrogen atoms were placed in calculated positions. The final cycle of full-matrix least-squares refinement on F^2 was based on 20380 reflections and 487 variable parameters

and converged. All refinements were performed using the ShelXL[1] via the OLEX2[2] interface. ORTEP diagrams were generated using PLATON. [3]

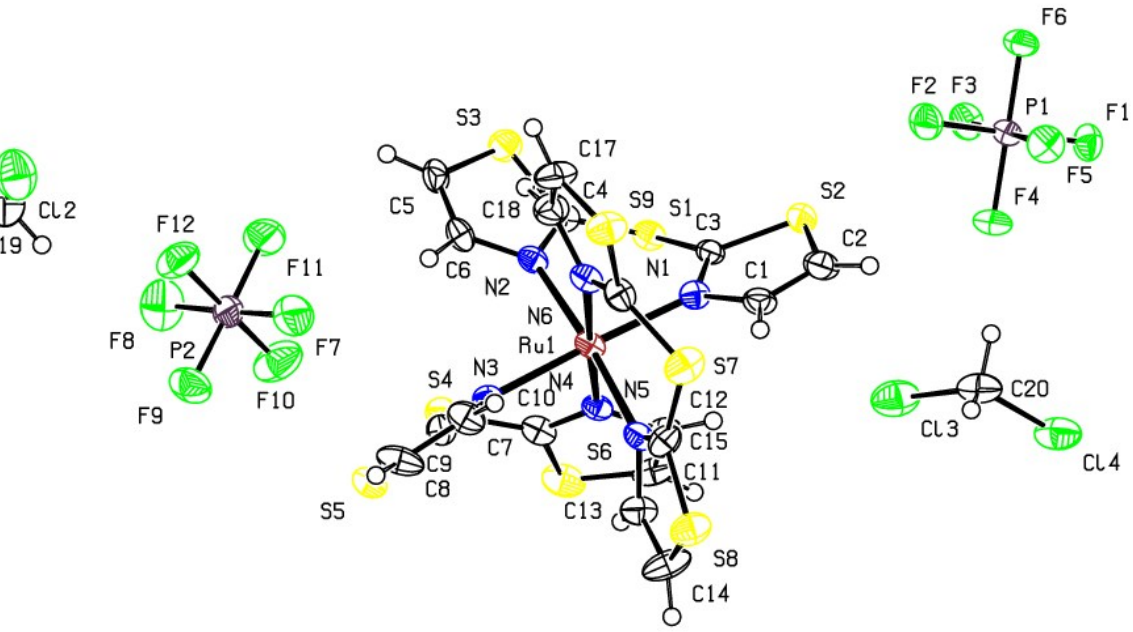

Figure S17. Asymmetric unit of **7** with thermal ellipsoids drawn are at 50 % probability level.

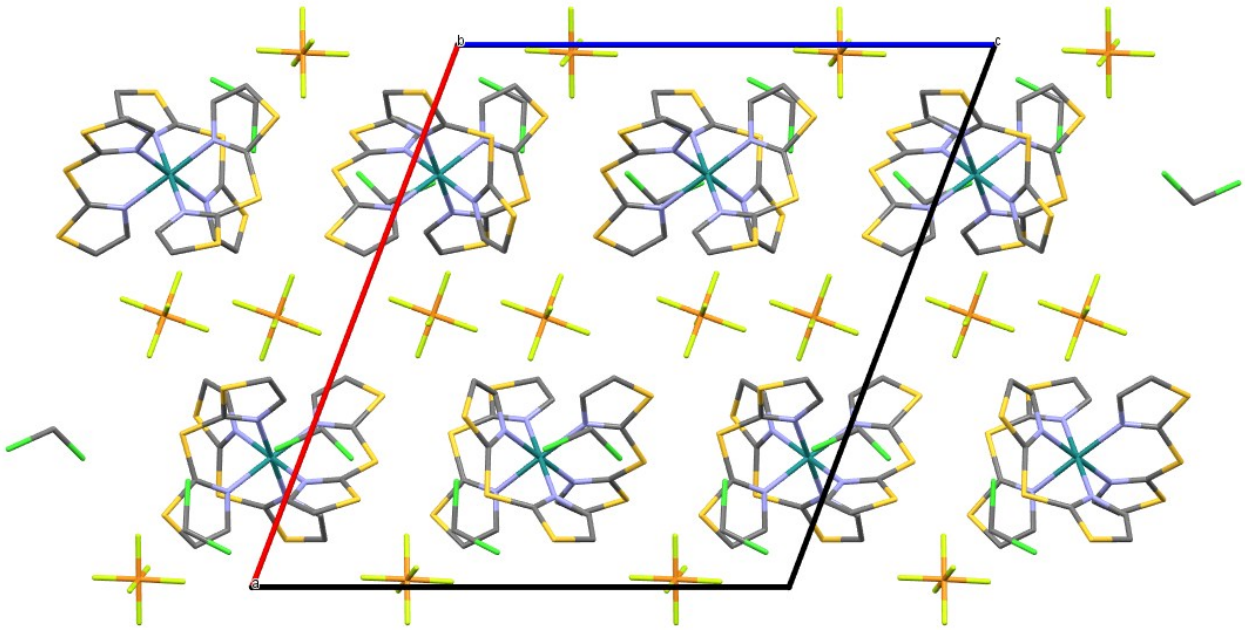

Figure S18. Packing diagram of **7** viewed along the b-axis. Hydrogen atoms are excluded for clarity.

$[Ru(tzSO_2)_2(MeCN)_2][PF_6]$ (**8**)

An orange plate shaped crystal of $C_{16}H_{14}F_{12}N_6O_4P_2RuS_6$, having approximate dimensions of 0.33 × 0.30 × 0.09 mm was mounted on a glass fiber. The data were collected at a temperature of -183.0 + 0.1°C to a maximum 2Θ value of 56.7°. Data were collected in a series of ϕ and ω scans in 0.5° oscillations using 10.0-second exposures. Of the 15144 reflections that were collected, 3639 were unique (Rint = 0.042); equivalent reflections were merged. All non-hydrogen atoms were refined anisotropically. All hydrogen atoms were placed in calculated positions. The final cycle of full-matrix least-squares refinement on F2 was based on 15144 reflections and 215 variable parameters and converged. All refinements were performed using the ShelXL[1] via the OLEX2[2] interface. ORTEP diagrams were generated using PLATON. [3]

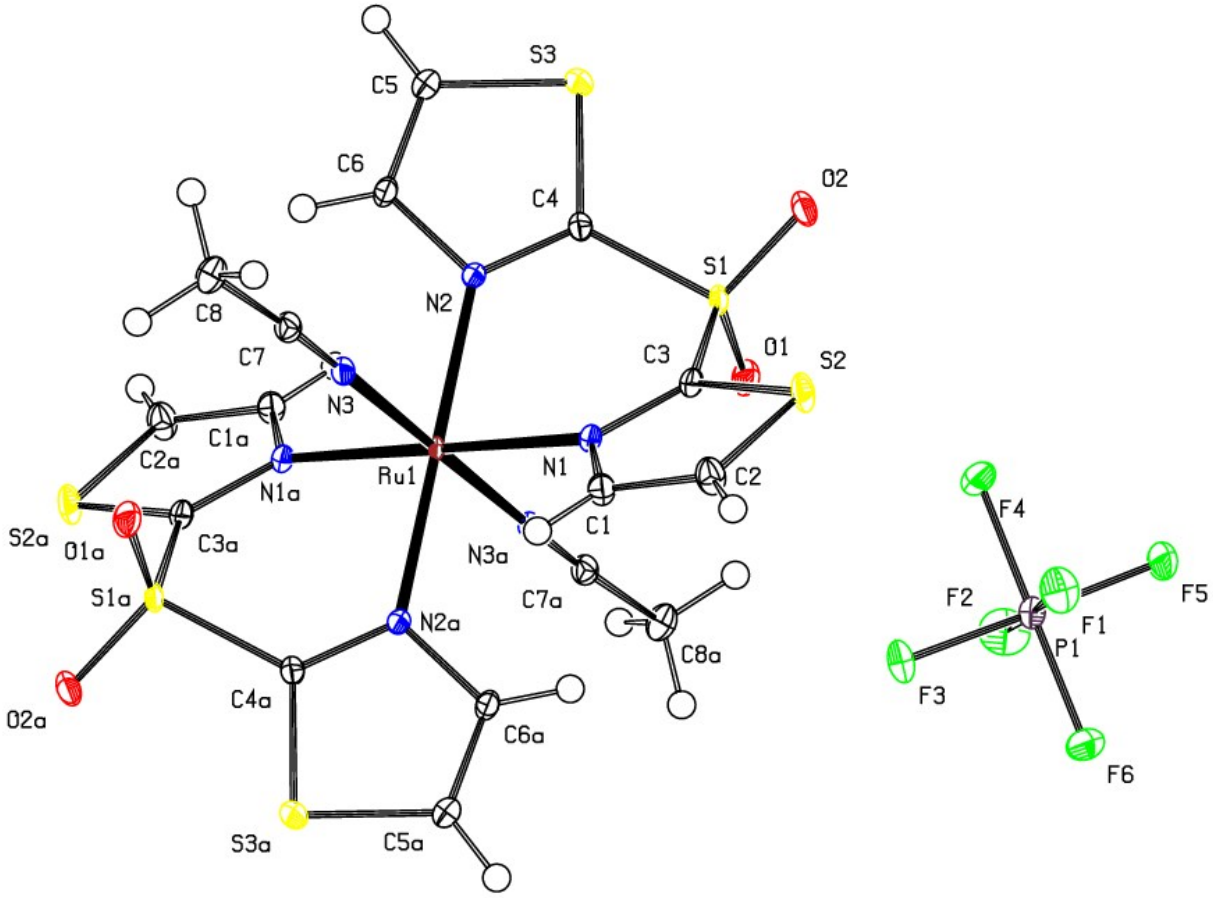

Figure S19. Asymmetric unit of **8** with thermal ellipsoids drawn are at 50 % probability level.

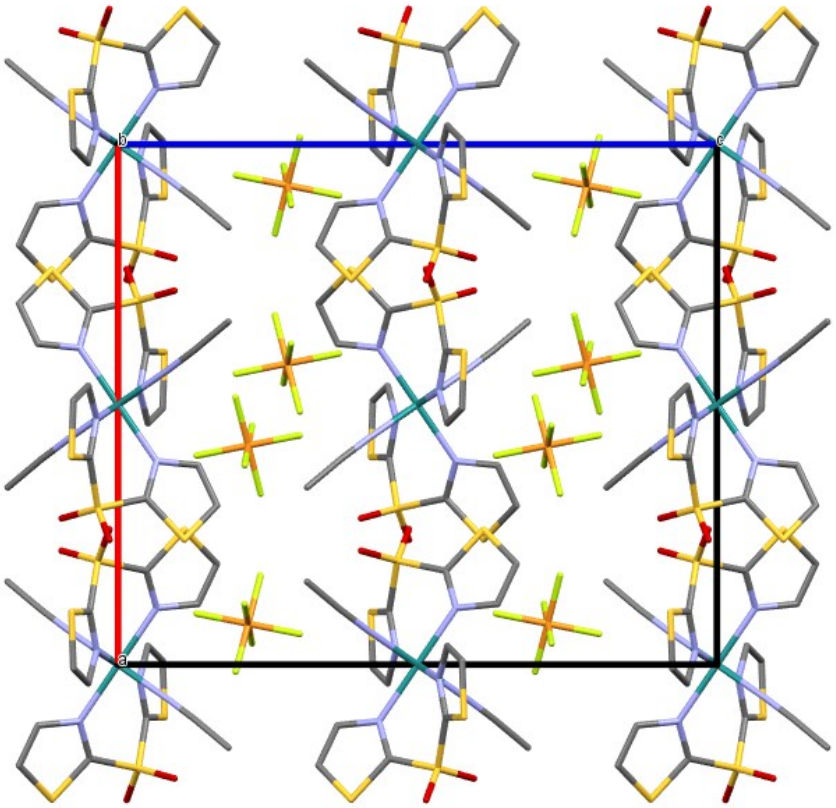

Figure S20. Packing diagram of **8** viewed along the b-axis. Hydrogen atoms are excluded for clarity.

$[Ru(bpy)_2(tzS)][PF_6]_2$ (**9**)

An orange prism shaped crystal of $C_{26}H_{20}F_{12}N_6P_2RuS_3$, having approximate dimensions of 0.123 × 0.101 × 0.09 mm was mounted on a nylon loop. The data were collected at a temperature of -183.0 + 0.1°C to a maximum 2Θ value of 56.6°. Data were collected in a series of ϕ and ω scans in 0.5° oscillations using 10.0-second exposures. Of the 30867 reflections that were collected, 8537 were unique (Rint = 0.024); equivalent reflections were merged. All non-hydrogen atoms were refined anisotropically. All hydrogen atoms were placed in calculated positions. The final cycle of full-matrix least-squares refinement on F^2 was based on 30867 reflections and 451 variable parameters and converged. All refinements were performed using the ShelXL[1] via the OLEX2[2] interface. ORTEP diagrams were generated using PLATON. [3]

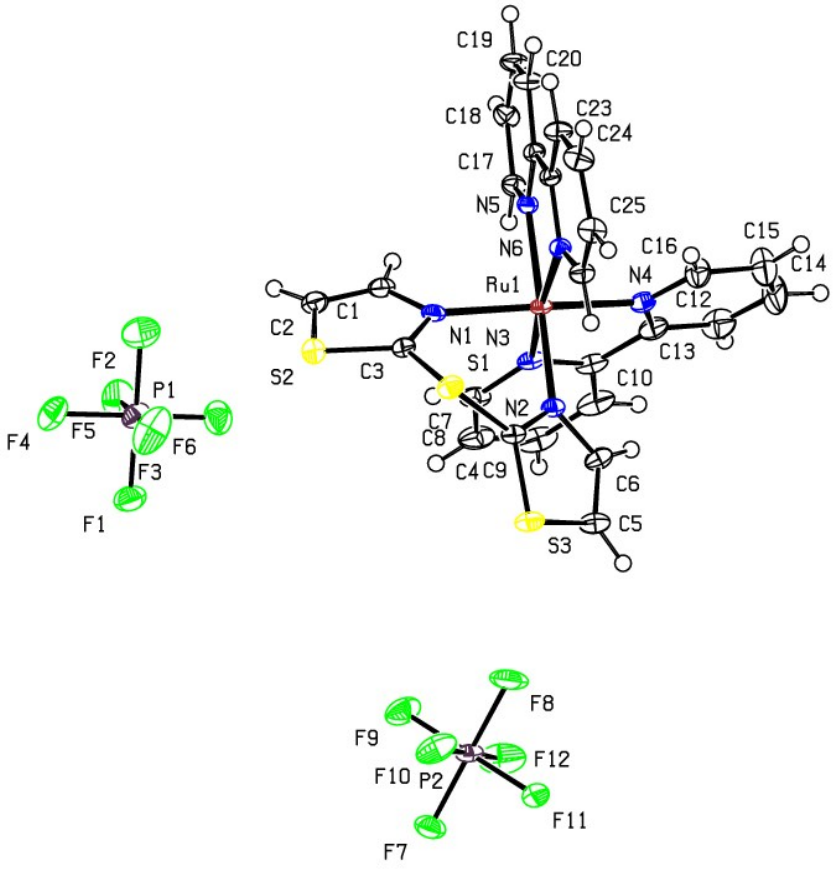

Figure S21. Asymmetric unit of **9** with thermal ellipsoids drawn are at 50 % probability level.

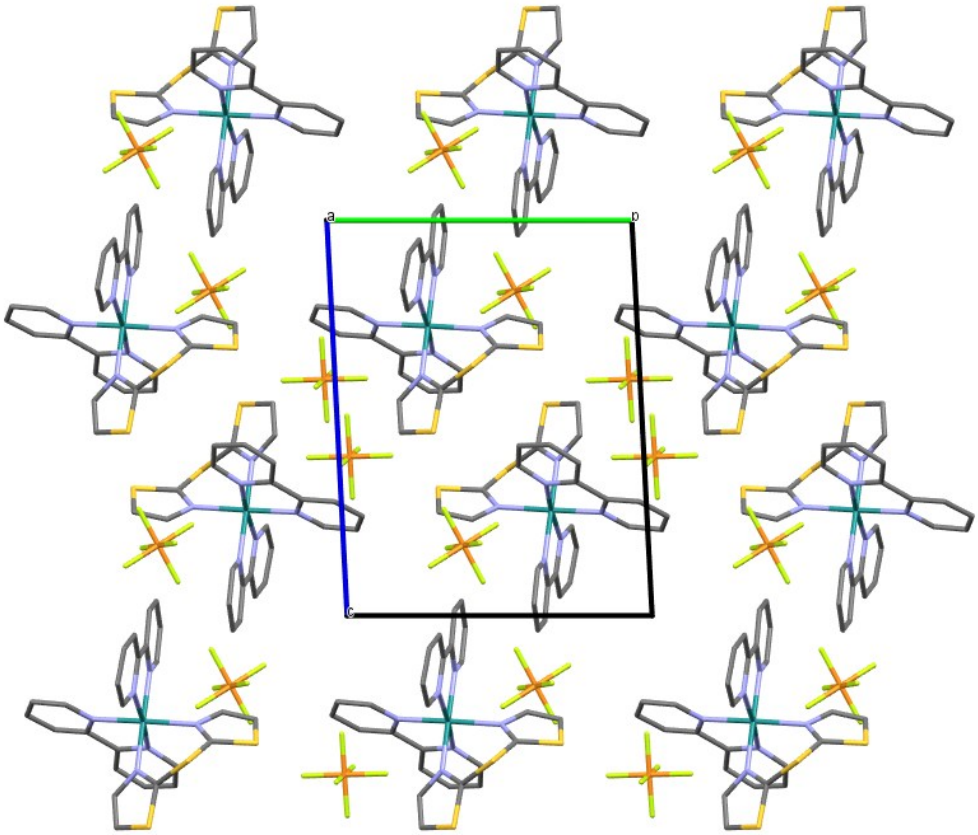

Figure S22. Packing diagram of **9** viewed along the a-axis. Hydrogen atoms are excluded for clarity.

$[Ru(phen)_2(tzSO_2)][PF_6]_2$ (**12**)

An orange plate shaped crystal of $C_{30}H_{20}F_{12}N_6O_2P_2RuS_3$, having approximate dimensions of 0.12 × 0.10 × 0.05 mm was mounted on a nylon loop. The data were collected at a temperature of -183.0 + 0.1°C to a maximum 2Θ value of 53.1°. Data were collected in a series of ϕ and ω scans in 0.5° oscillations using 10.0-second exposures. Of the 31751 reflections that were collected, 7421 were unique (Rint = 0.039); equivalent reflections were merged. One of the PF_6 anions are disordered and was modeled in two orientations. A series of SADI commands were used to ensure reasonable geometries and displacement parameters. A list of the constraints and restraints used in this refinement can be found within the CIF. All non-hydrogen atoms were refined anisotropically. All hydrogen atoms were placed in calculated positions. The final cycle of full-matrix least-squares refinement on F^2 was based on 31751 reflections and 569 variable parameters and converged. All

refinements were performed using the ShelXL[1] via the OLEX2[2] interface. ORTEP diagrams were generated using PLATON. [3]

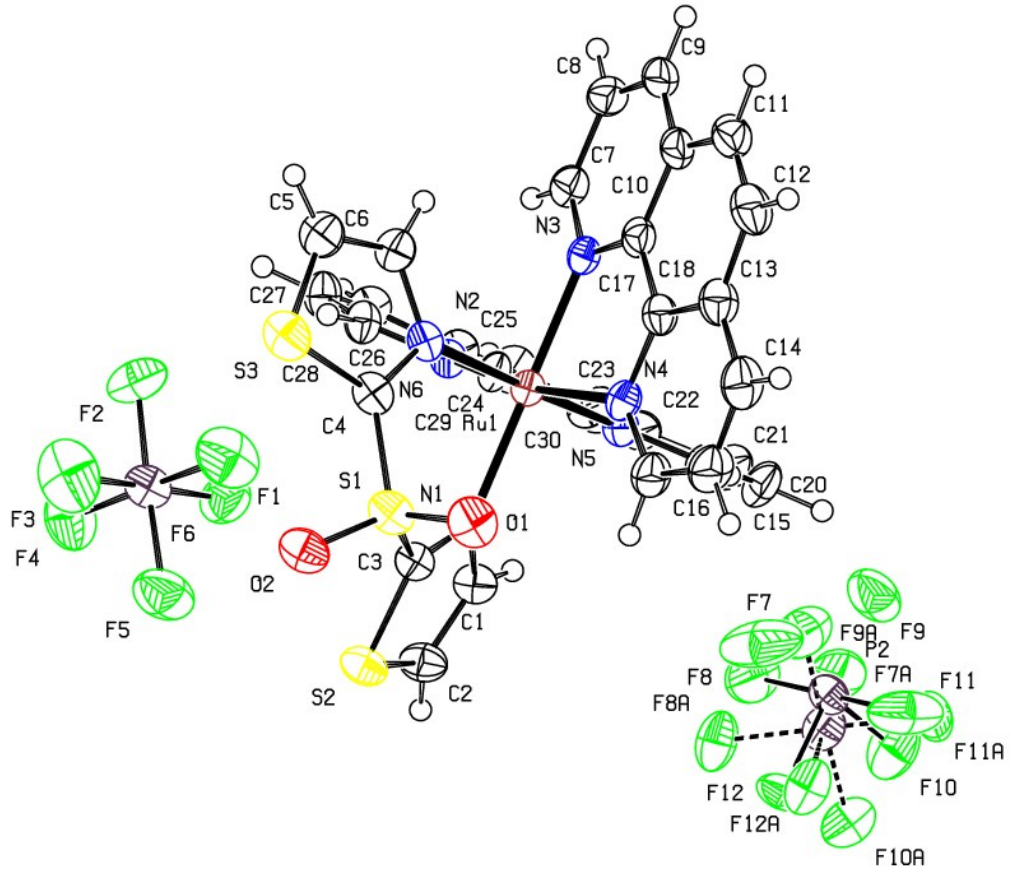

Figure S23. Asymmetric unit of **12** with thermal ellipsoids drawn are at 50 % probability level.

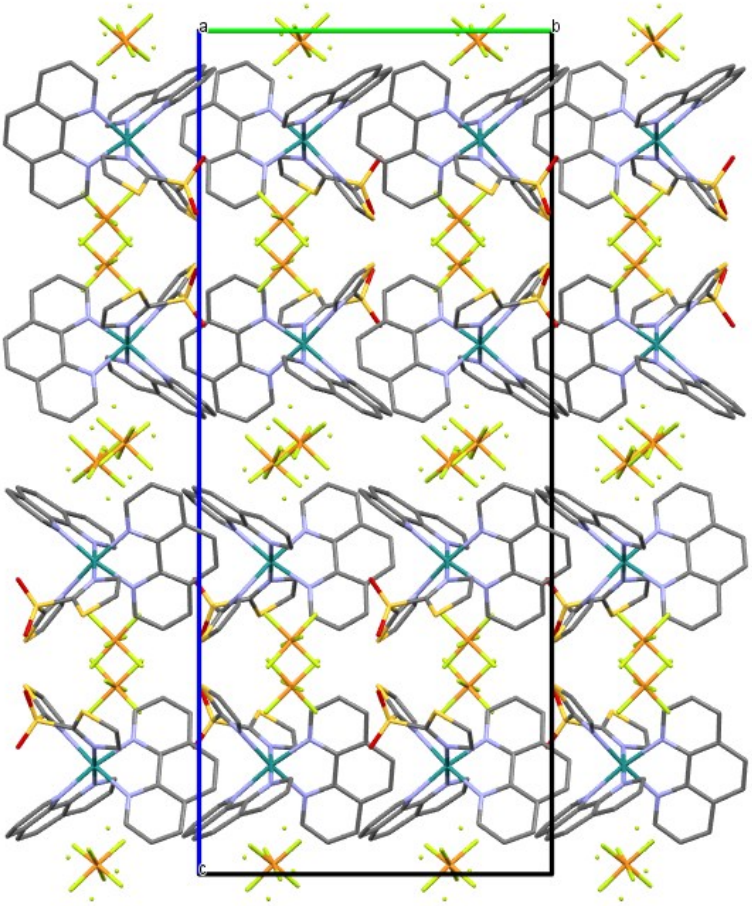

Figure S24. Packing diagram of **12** viewed along the a-axis. Minor disordered fragments are shown as points. Hydrogen atoms are excluded for clarity.

Copper(I) Complexes

[Cu(POP)tzS][BF_4]$_2$ (**13)**

A yellow prism shaped crystal of $C_{42}H_{32}BCuF_4N_2OP_2S_3$▪$CH_2Cl_2$/$(C_2H_5)_2O$, having approximate dimensions of 0.38 × 0.11 × 0.02 mm was mounted on a nylon loop. The data were collected at a temperature of -183.0 + 0.1°C to a maximum 2Θ value of 52.8°. Data were collected in a series of ϕ and ω scans in 0.5° oscillations using 10.0-second exposures. Of the 68044 reflections that were collected, 17006 were unique (Rint = 0.032); equivalent reflections were merged. The material crystallized with two molecules in the asymmetric unit and with a CH_2Cl_2 and $(C_2H_5)_2O$ molecule occupying the same space in the asymmetric unit. Additionally, one BF_4 anion is disordered and was modeled in two orientations. A series of SADI commands were used to ensure reasonable geometries and displacement parameters. A list of the constraints and restraints used in this refinement can be found within the CIF. All non-hydrogen atoms were refined anisotropically. All hydrogen atoms were placed in calculated positions. The final cycle of full-matrix least-squares refinement on F^2 was based on 68044 reflections and 1121 variable parameters and converged. All refinements were performed using the ShelXL[1] via the OLEX2[2] interface. ORTEP diagrams were generated using PLATON. [3]

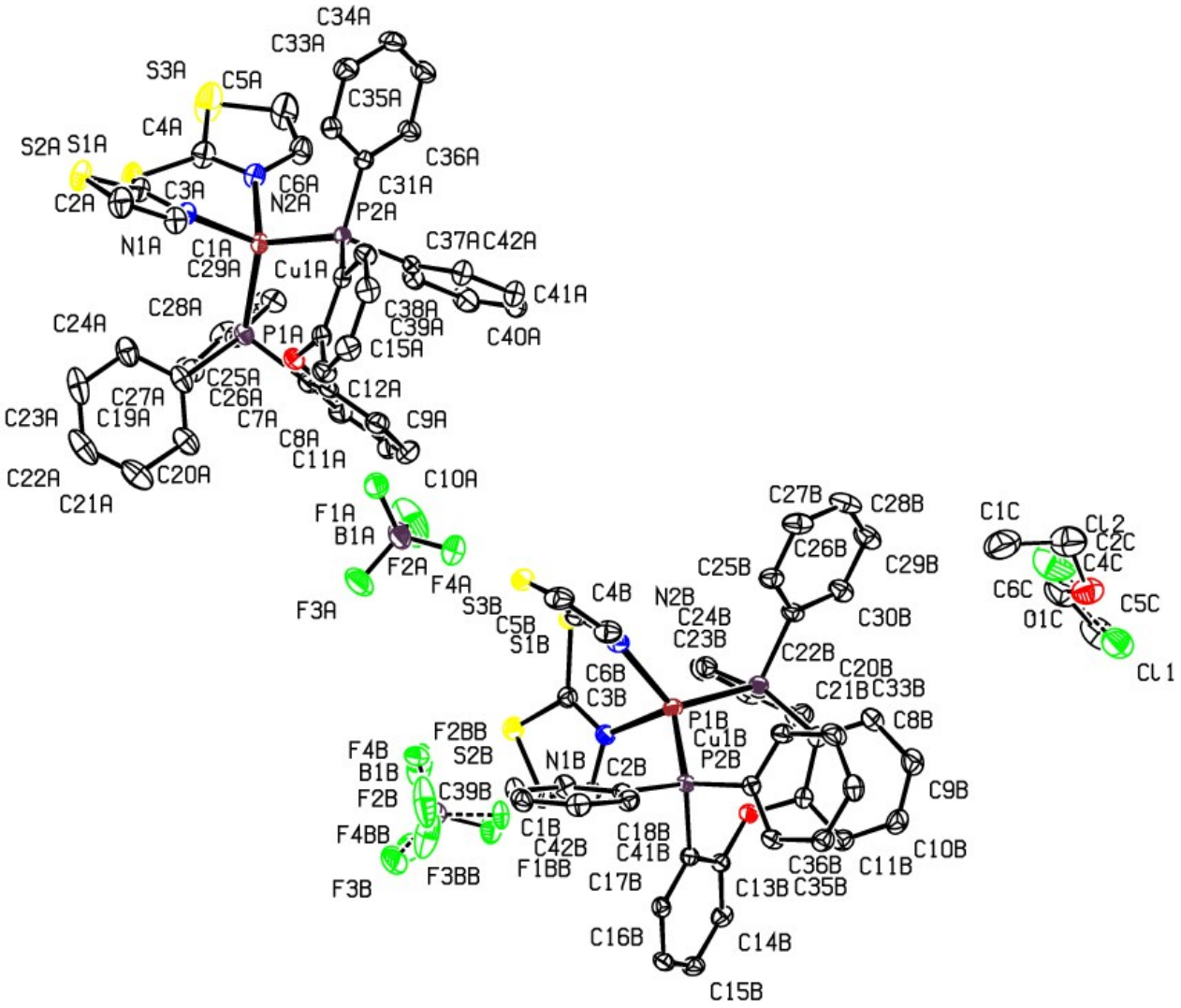

Figure S25. Asymmetric unit of **13** with thermal ellipsoids drawn are at 50 % probability level. Hydrogen atoms are excluded for clarity.

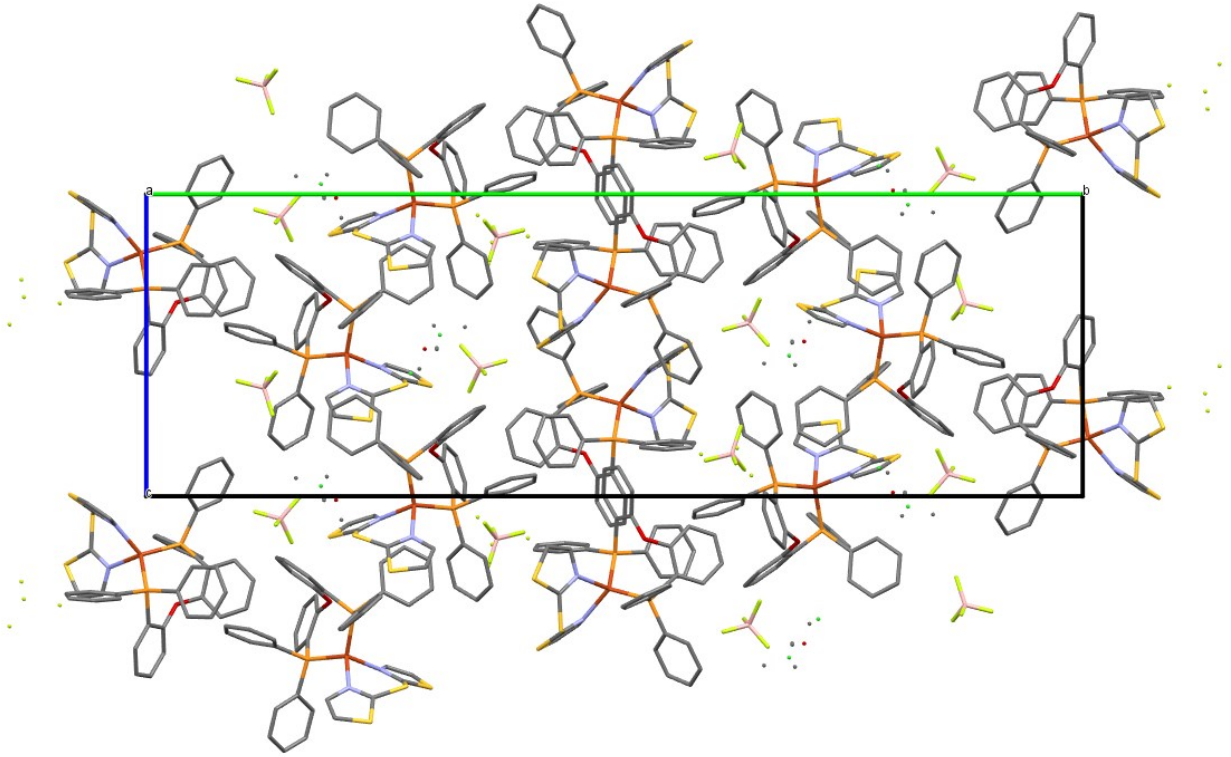

Figure S26. Packing diagram of **13** viewed along the a-axis. Minor disordered fragments are shown as points. Hydrogen atoms are excluded for clarity.

[Cu(POP)tzSO_2][BF_4] (**14**)

A yellow prism shaped crystal of $C_{41}H_{32}BCuF_4N_2O_3P_2S_3$▪$CH_2Cl_2$, having approximate dimensions of 0.41 × 0.21 × 0.11 mm was mounted on a nylon loop. The data were collected at a temperature of -183.0 + 0.1°C to a maximum 2Θ value of 56.0°. Data were collected in a series of ϕ and ω scans in 0.5° oscillations using 10.0-second exposures. Of the 30265 reflections that were collected, 10029 were unique (Rint = 0.0215); equivalent reflections were merged. The material crystallized with one molecule of CH_2Cl_2 in the asymmetric unit. Additionally, the BF_4 anion is disordered and was modeled in two orientations. A series of SADI commands were used to ensure reasonable geometries and displacement parameters. A list of the constraints and restraints used in this refinement can be found within the CIF. All non-hydrogen atoms were refined anisotropically. All hydrogen atoms were placed in calculated positions. The final cycle of full-matrix least-squares refinement on F^2 was based on 30265 reflections and 560 variable parameters and converged. All refinements were performed using the ShelXL[1] via the OLEX2[2] interface. ORTEP diagrams were generated using PLATON. [3]

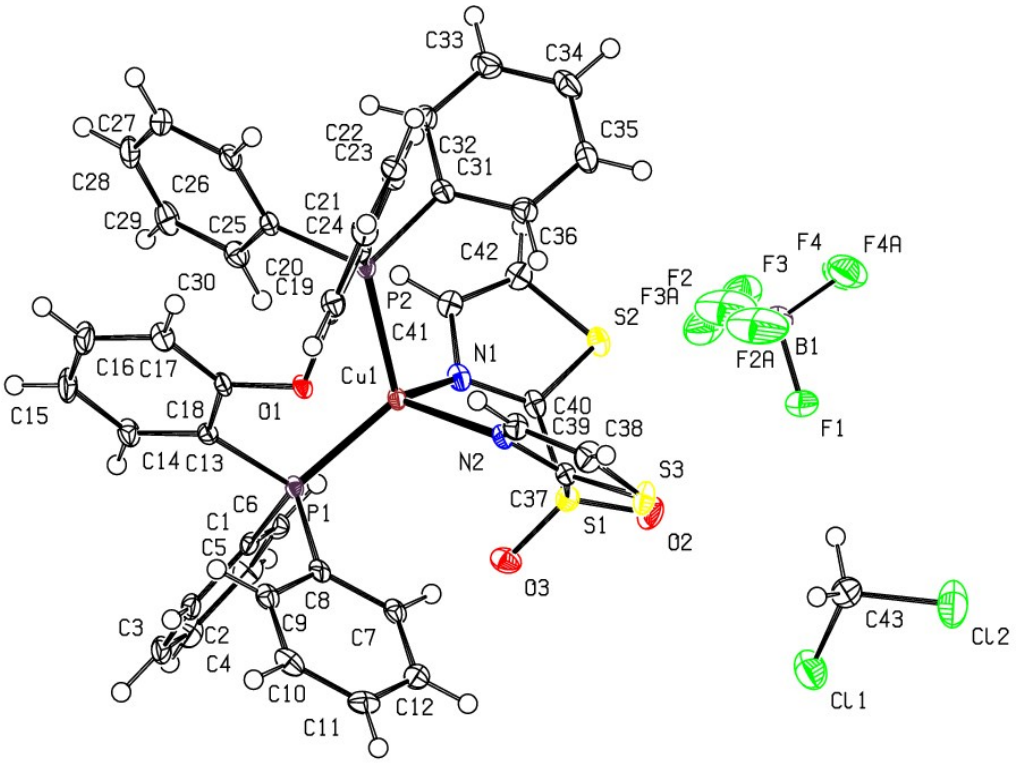

Figure S27. Solvated asymmetric unit of **14** with thermal ellipsoids drawn are at 50 % probability level.

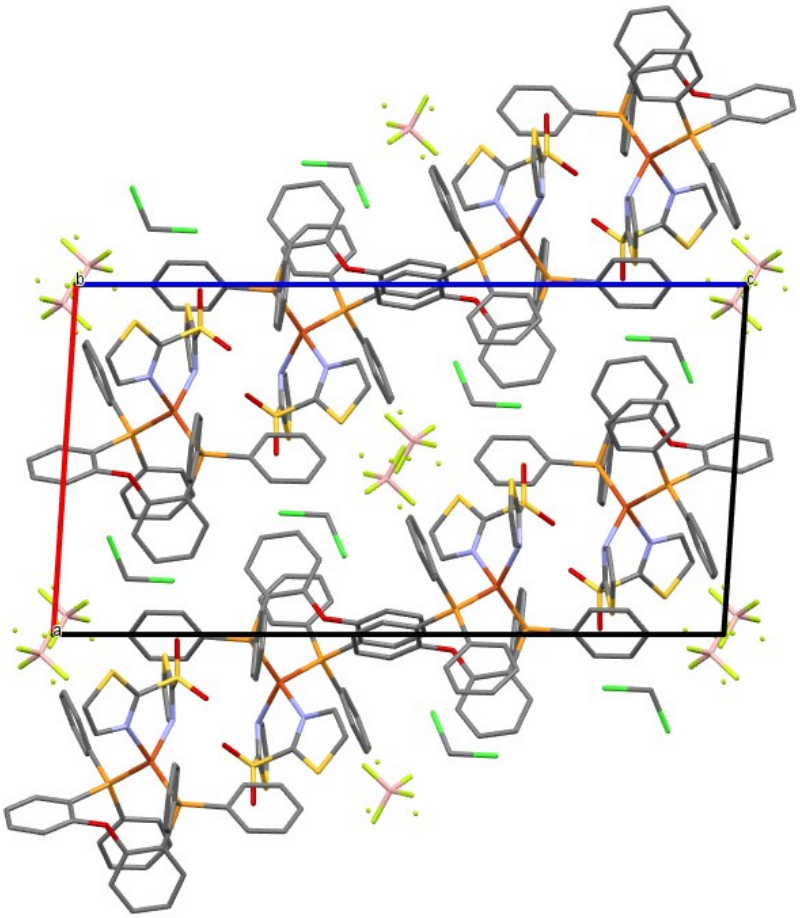

Figure S28. Packing diagram of **14** viewed along the b-axis. Minor disordered fragments are shown as points. Hydrogen atoms are excluded for clarity.

[Cu(POP)(hbtz)][BF_4] (**15**)

A yellow prism shaped crystal of $C_{90}H_{84}BCu_2F_4N_2O_2P_4S_2 \cdot (C_2H_5)_2O$, having approximate dimensions of 0.31 × 0.26 × 0.23 mm was mounted on a glass fiber. The data were collected at a temperature of -183.0 + 0.1°C to a maximum 2Θ value of 56.7°. Data were collected in a series of ϕ and ω scans in 0.5° oscillations using 10.0-second exposures. Of the 30305 reflections that were collected, 11409 were unique (Rint = 0.020); equivalent reflections were merged. The material crystallized with 1 molecule of $(C_2H_5)_2O$ in the asymmetric unit, which is disordered and modeled in two orientations. Additionally, the terminal CH_2 and CH_3 atoms in hexyl chain are disordered over three orientations. Finally, the BF_4 anion is disordered and was modeled in two orientations. A series of SADI commands were used to ensure reasonable geometries and displacement parameters. A list of the constraints and restraints used in this refinement can be found within the

CIF. All non-hydrogen atoms were refined anisotropically. All hydrogen atoms were placed in calculated positions. The final cycle of full-matrix least-squares refinement on F^2 was based on 30305 reflections and 696 variable parameters and converged. All refinements were performed using the ShelXL[1] via the OLEX2[2] interface. ORTEP diagrams were generated using PLATON. [3]

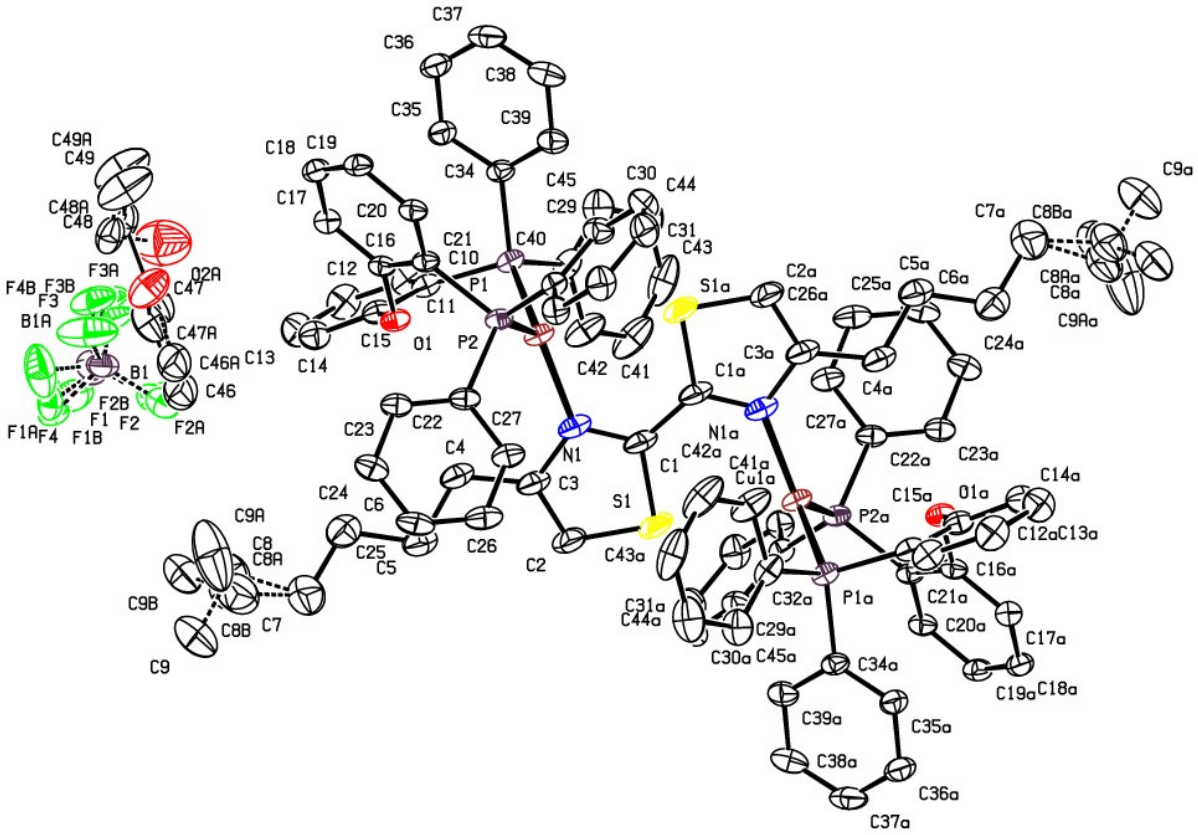

Figure S29. Dimeric unit of **15** with thermal ellipsoids drawn are at 50 % probability level. Hydrogen atoms are excluded for clarity.

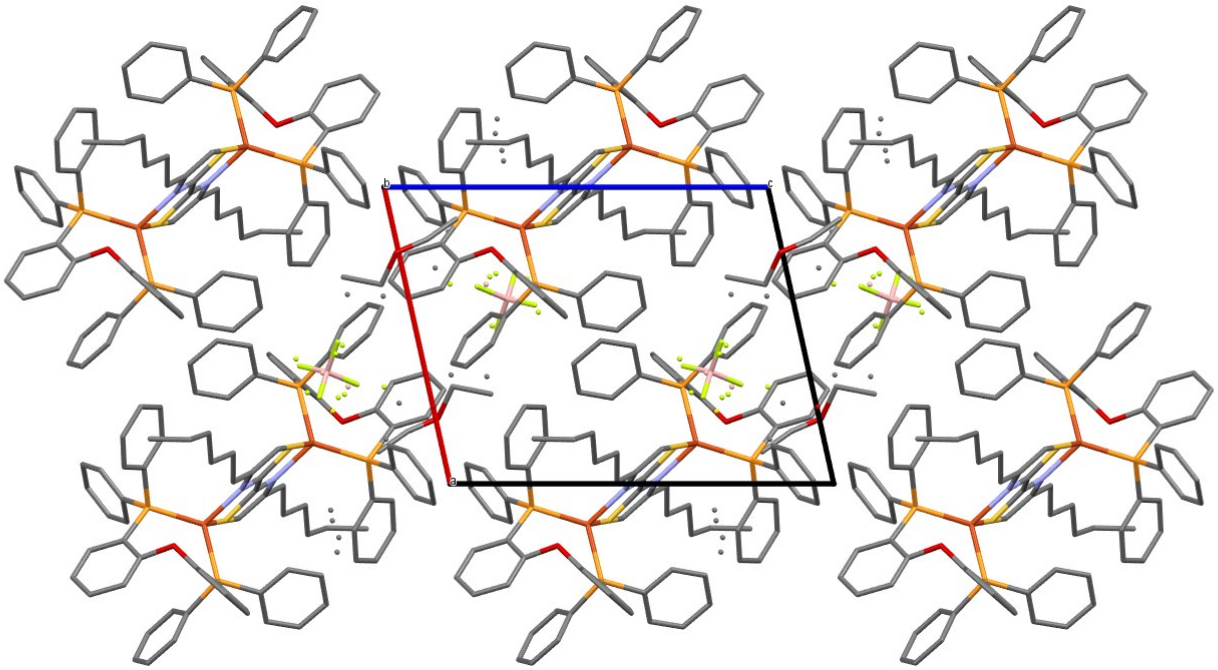

Figure S30. Packing diagram of **15** viewed along the b-axis. Minor disordered fragments are shown as points. Hydrogen atoms are excluded for clarity.

SPECTROSCOPIC DATA

Ruthenium(II) Complexes

Absorption Spectroscopy

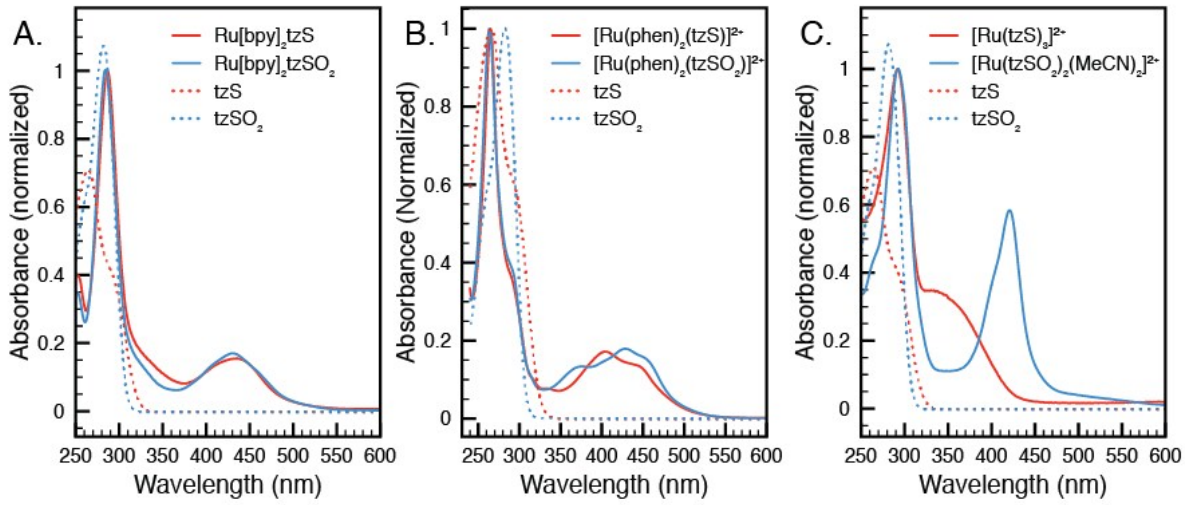

Figure S31. UV-vis absorption spectra of Ru(II) complexes (solid traces) and pro-ligands (dashed traces) at 293 K. (a) tzS (**5**), $tzSO_2$ (**6**), $[Ru(bpy)_2(tzS)]^{2+}$ (**9**), and $[Ru(bpy)_2(tzSO_2)]^{2+}$ (**10**) in CH_2Cl_2; (b) **5**, **6**, $[Ru(phen)_2(tzS)]^{2+}$ (**11**) and $[Ru(phen)_2(tzSO_2)]^{2+}$ (**12**) in CH_2Cl_2, and (c) **5**, **6**, $[Ru(tzS)_3]^{2+}$ (**7**) and $[Ru(tzSO_2)_2(CH_3CN)_2]^{2+}$ (**8**) in CH_3CN.

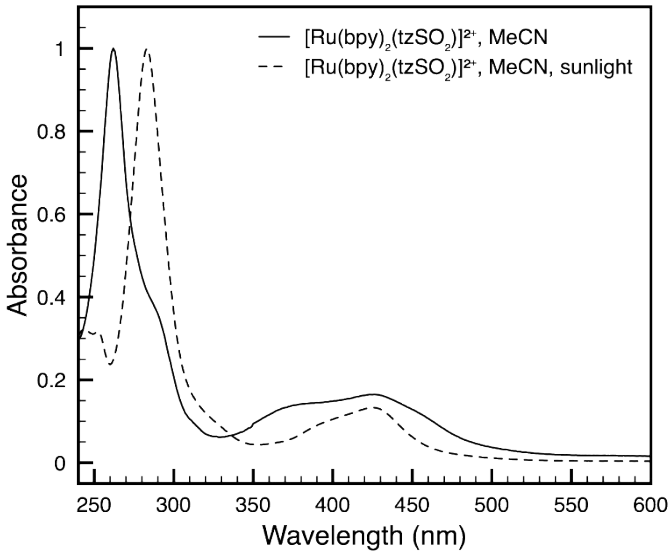

Figure S32. Absorbance of $[Ru(bpy)_2(tzSO_2)]^{2+}$ (**10**) in CH_3CN in the dark (solid trace) and after sunlight irradiation for 72 h (dashed trace) at 293 K.

Photoluminescence Spectroscopy

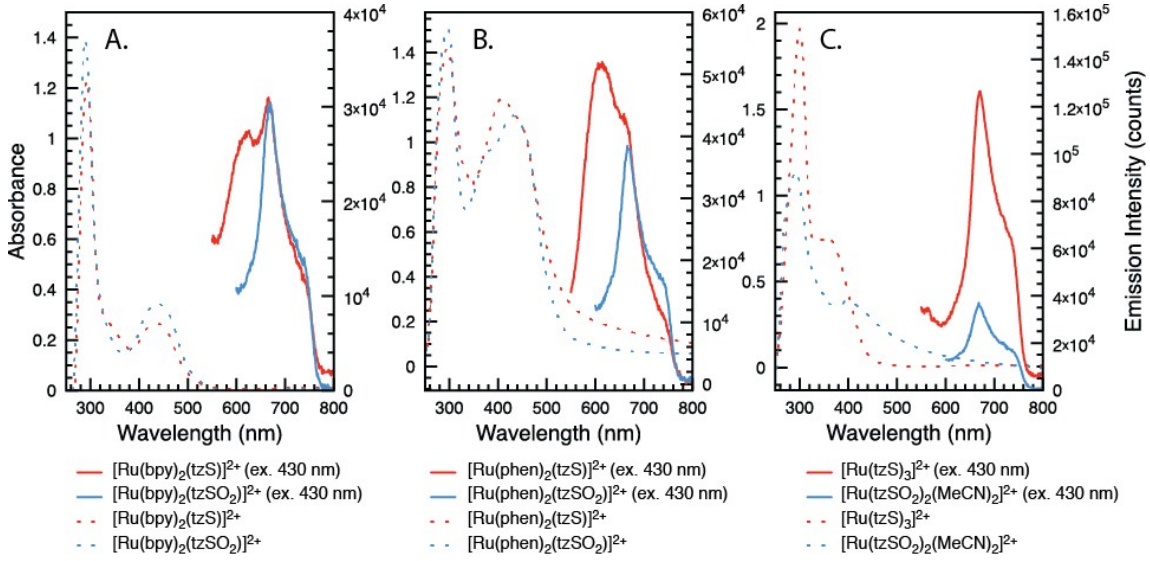

Figure S33. Absorption (dashed trace) and emission (solid trace) spectra of ruthenium(II) complexes (a) $[Ru(bpy)_2(tzS)]^{2+}$ (**9**) and $[Ru(bpy)_2(tzSO_2)]^{2+}$ (**10**); (b) $[Ru(phen)_2(tzS)]^{2+}$ (**11**) and $[Ru(phen)_2(tzSO_2)]^{2+}$ (**12**); (c) $[Ru(tzS)_3]^{2+}$ (**7**) and $[Ru(tzSO_2)_2(CH_3CN)_2]^{2+}$ (**8**). Neat thin films drop-cast from CH_2Cl_2 at 293 K.

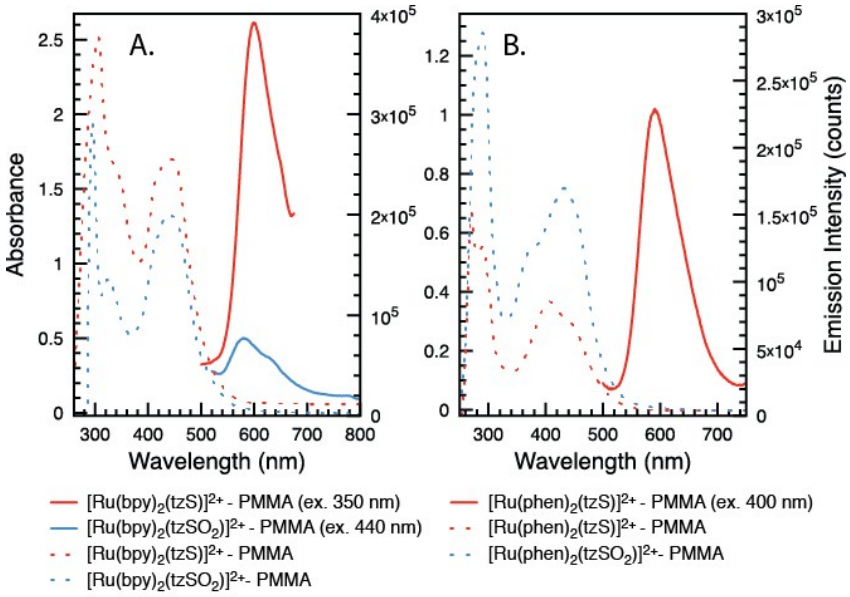

Figure S34. Absorption and emission of Ru(II) complexes (a) $[Ru(bpy)_2(tzS)]^{2+}$ (**9**) and $[Ru(bpy)_2(tzSO_2)]^{2+}$ (**10**); and (b) $[Ru(phen)_2(tzS)]^{2+}$ (**11**) and $[Ru(phen)_2(tzSO_2)]^{2+}$ (**12**). Doped in PMMA films drop-cast from CH_2Cl_2 at 293 K.

Table S8. Maximum emission wavelength for Ru(II) complexes **7**–**12** at room temperature as solid and in polymer matrix and 77 K for selected compounds.

	Thin film[a] λ_{max} (nm)		PMMA Matrix[a] λ_{max} (nm)
	293 K	77 K	
$[Ru(tzS)_3]^{2+}$ (**7**)	671 (735)	*b*	*b*
$[Ru(tzSO_2)_2(MeCN)_2]^{2+}$ (**8**)	668 (735)	*b*	*b*
$[Ru(bpy)_2(tzS)]^{2+}$ (**9**)	626; 666; (725)	615	599
$[Ru(bpy)_2(tzSO_2)]^{2+}$ (**10**)	669; (725)	652	581; (627)
$[Ru(phen)_2(tzS)]^{2+}$ (**11**)	615; (659); (740)	*b*	591
$[Ru(phen)_2(tzSO_2)]^{2+}$ (**12**)	667; (730)	*b*	*b*

a. drop-cast from CH_2Cl_2; *b*. not attempted; ( ) shoulders

Electrochemical Data

Table S9. Redox potentials of ruthenium(II) complexes (**7–12**) and selected literature complexes *vs*. NHE along with the electrochemical and optical band gaps.

			E_g [eV]	
	E_{ox} (Ru^{3+}/Ru^{2+}) [V]	E_{red} [V]	Echem	Optical
$[Ru(bpy)_3]^{2+}$ [4]	1.54	–1.08; –1.27; –1.51; –2.15	2.62	–
$[Ru(phen)_3]^{2+}$ [4]	1.61	–1.19; –1.29; –1.59; –1.99	2.80	–
$[Ru(btz)_3]^{2+}$ [5]	1.11	–0.79; –1.00; –1.26	1.90	–
$[Ru(bpy)_2(btz)]^{2+}$ [5]	1.56	–0.84; –1.20; –1.42	2.40	–
$[Ru(tzS)_3]^{2+}$ (**7**)	1.62	–0.75; –1.23	2.19	2.75
$[Ru(tzSO_2)_2(MeCN)_2]^{2+}$ (**8**)	0.95	–0.80; –1.09	1.75	2.47
$[Ru(bpy)_2(tzS)]$ (**9**)	1.52	–0.74; –1.31; –1.58	2.26	2.27
$[Ru(bpy)_2(tzSO_2)]^{2+}$ (**10**)	1.88	–0.57; –0.78	2.45	2.27
$[Ru(phen)_2(tzS)]^{2+}$ (**11**)	1.59	–0.71; –1.04	2.30	2.28
$[Ru(phen)_2(tzSO_2]^{2+}$ (**12**)	1.63	–0.85	2.48	2.28

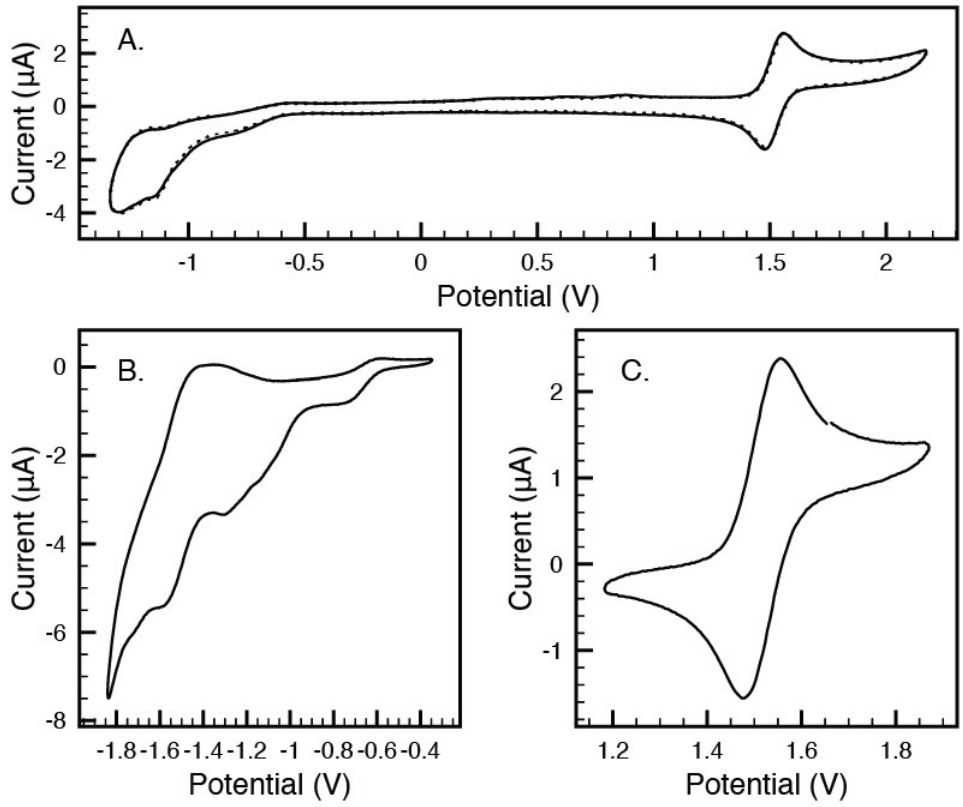

Figure S35. Cyclic voltammetry of $[Ru(bpy)_2(tzS)][PF_6]_2$ (**9**) in 0.1 M NBu_4PF_6 CH_3CN solutions using a platinum working electrode vs. NHE at 293 K.

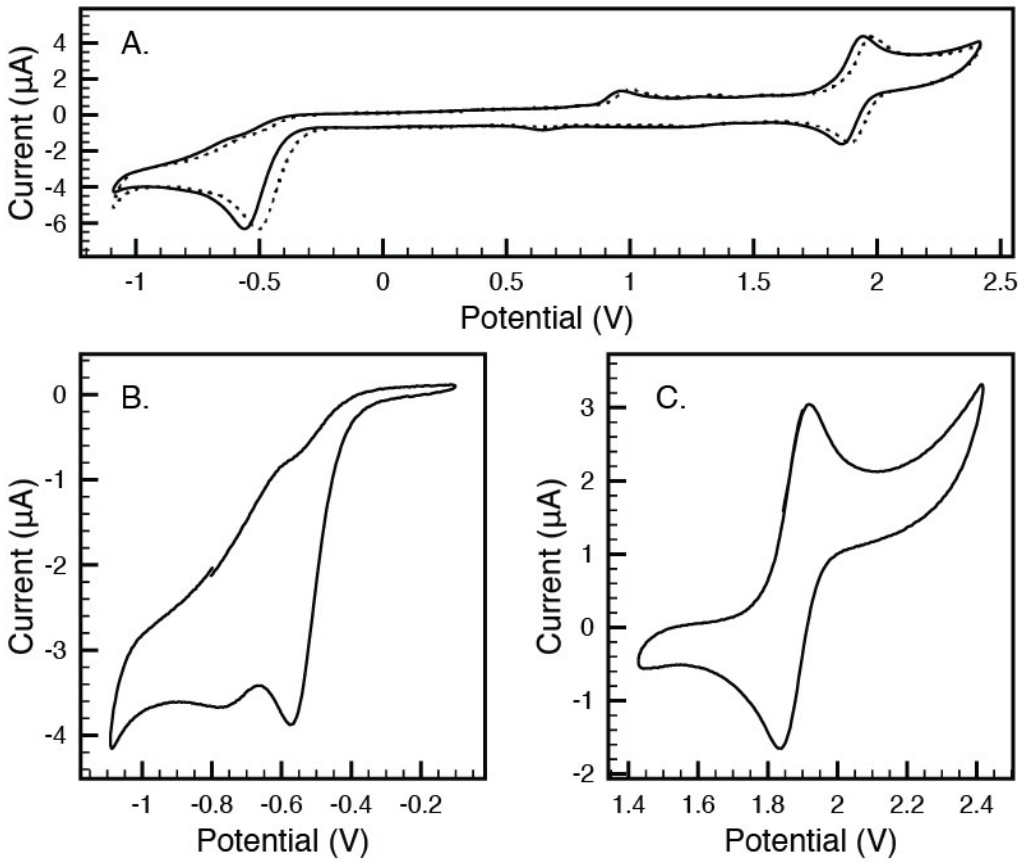

Figure S36. Cyclic voltammetry of **[**$Ru(bpy)_2(tzSO_2)][PF_6]_2$ (**10**) in 0.1 M NBu_4PF_6 CH_3CN solutions using platinum working electrode vs. NHE at 293 K.

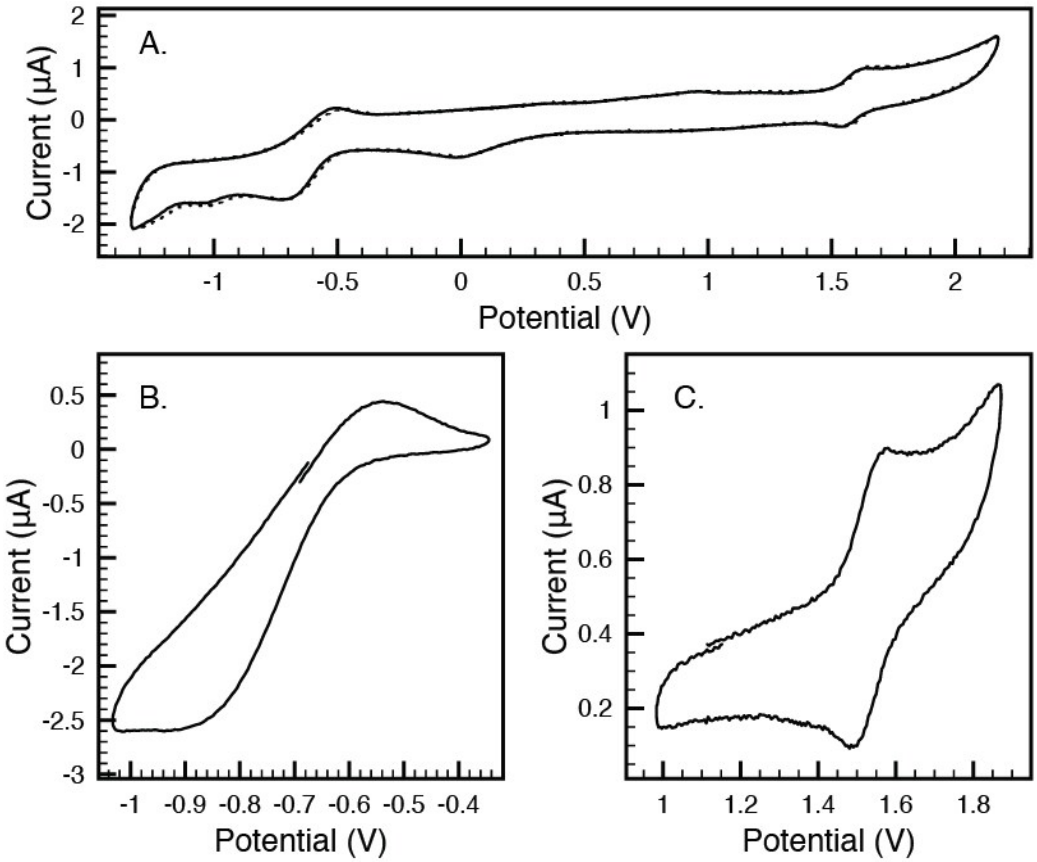

Figure S37. Cyclic voltammetry of $[Ru(phen)_2(tzS)][PF_6]_2$ (**11**) in 0.1 M NBu_4PF_6 CH_3CN solutions using platinum working electrode vs. NHE at 293 K.

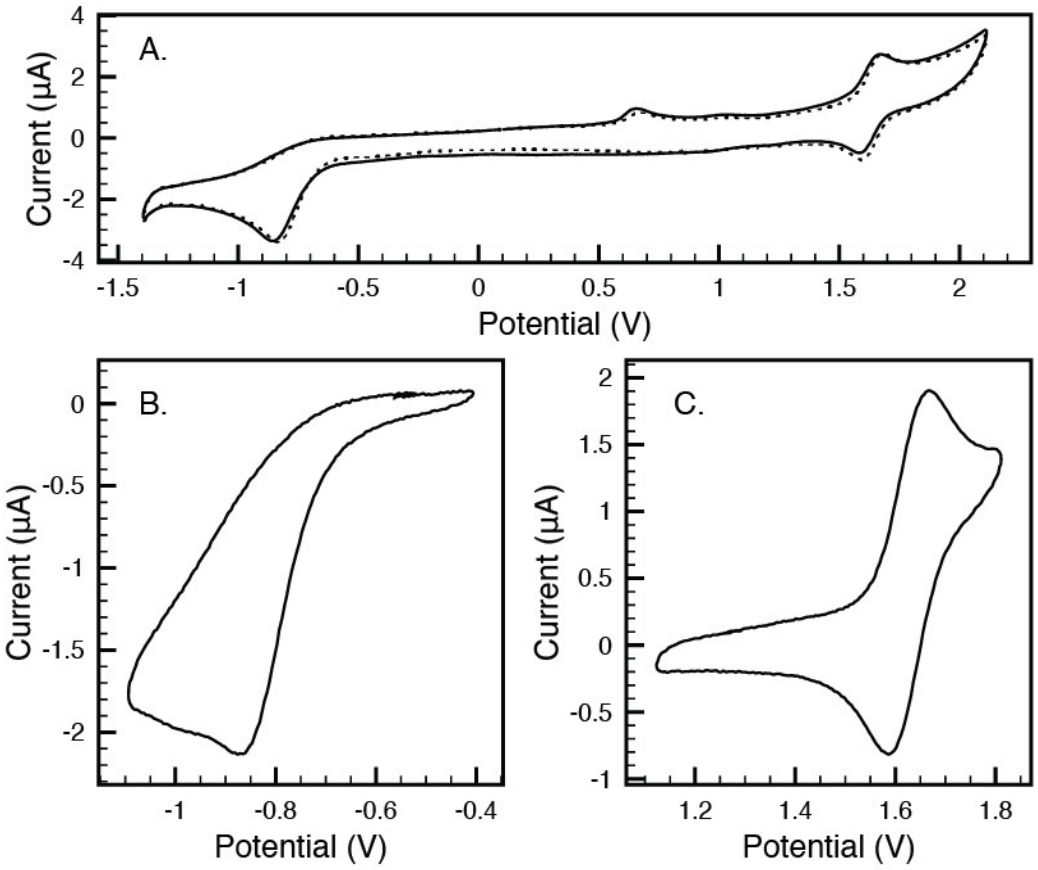

Figure S38. Cyclic voltammetry of $[Ru(phen)_2(tzSO_2)][PF_6]_2$ (**12**) in 0.1 M NBu_4PF_6 CH_3CN solutions using platinum working electrode vs. NHE at 293 K.

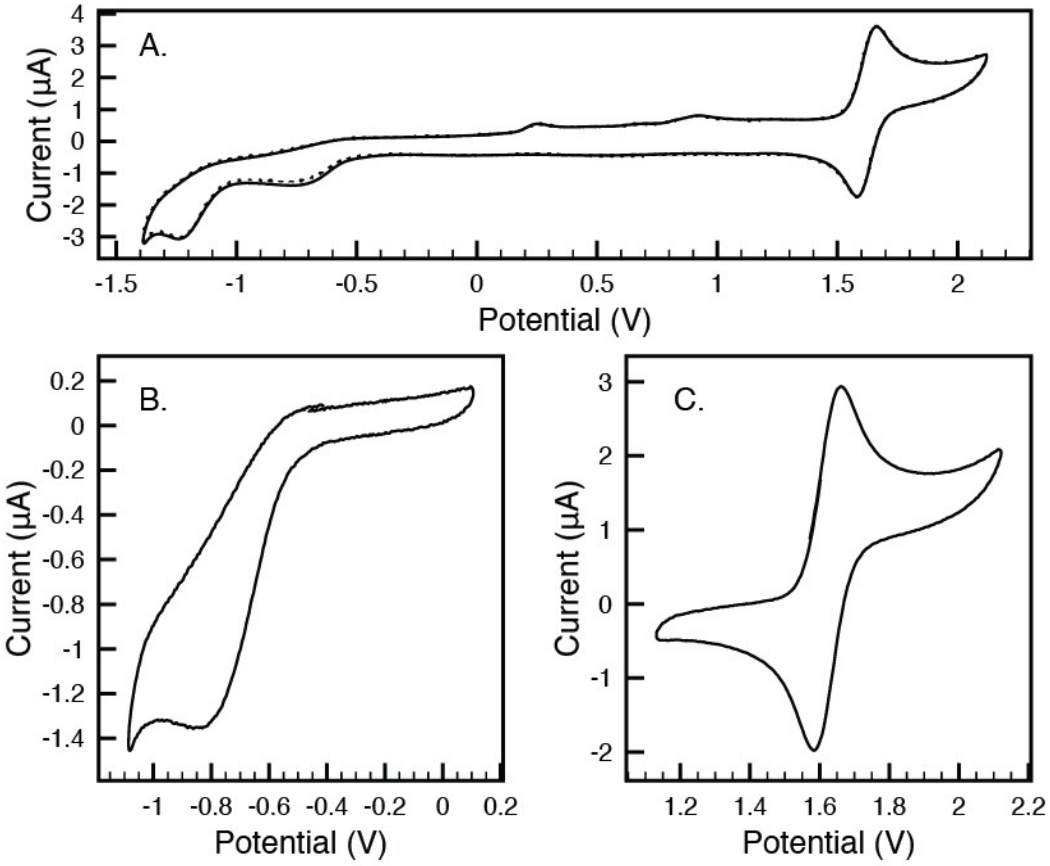

Figure S39. Cyclic voltammetry of $[Ru(tzS)_3][PF_6]_2$ (**7**) in 0.1 M $NBu_4PF_6CH_3CN$ solutions using platinum working electrode vs. NHE at 293 K.

Copper(I) Complexes

Absorption Spectroscopy

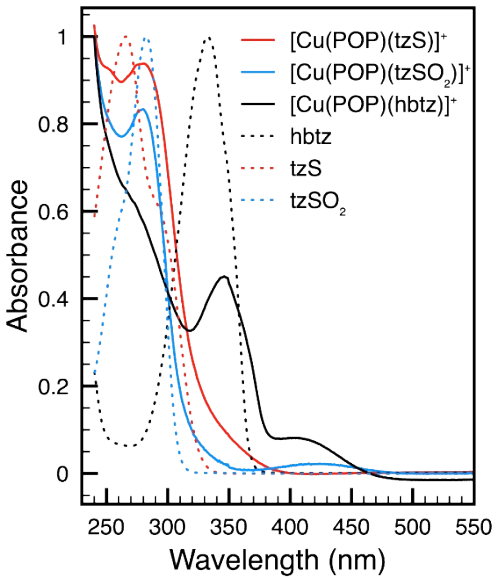

Figure S40. Absorption spectra of the Cu(I) complexes (solid traces) $[Cu(POP)(tzS)]^+$ (**13**); $[Cu(POP)(tzSO_2)]^+$ (**14**); $[(POP)Cu(hbtz)Cu(POP)]^{2+}$ (**15**); and pro-ligands (dashed traces) tzS (**5**); $tzSO_2$ (**6**); and **hbtz.** CH_2Cl_2 solutions at 293 K.

Photoluminescence Spectroscopy

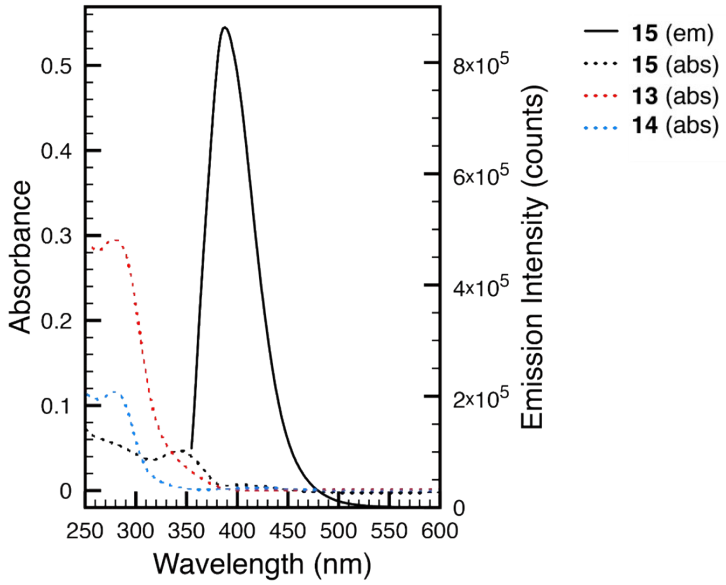

Figure S41. Absorption (dashed trace) and emission (solid trace) of Cu(I) species in CH_2Cl_2 solutions. ***13** and **14** were found to be non-emissive in solution.

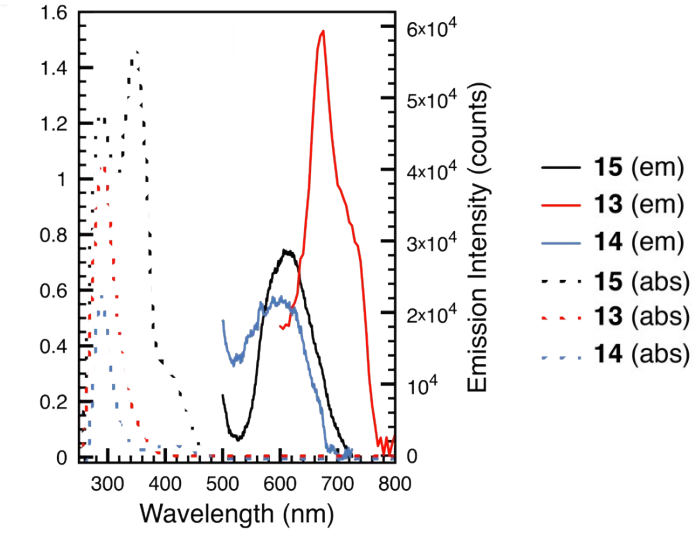

Figure S42. Absorption (dashed trace) and emission (solid trace) spectra of Cu(I) complexes doped in a PMMA matrix. All films drop-cast from CH_2Cl_2 and spectra collected at 293 K with λ_{ex} = 405 nm for (Except $[Cu(POP)(tzS)]^+$ (**13**) in PMMA: λ_{ex} = 430 nm)**.**

Electrochemical Data

Table S10. Electrochemical potentials (vs. NHE) of copper(I) complexes (**13**–**15**) measured in 0.1 M NH_4PF_6 CH_3CN solutions at 293 K.

	E_{ox} (V)	E_{red} (V)	Eg (eV)	
			Echem	Optical
$[Cu(POP)(tzS)]^+$ (**13**)	1.67; 0.94	–0.86	2.53	3.12
$[Cu(POP)(tzSO_2)]^+$ (**14**)	1.56	–1.32	2.84	2.56
$[Cu(POP)(hbtz)]^+$ (**15**)	1.89	–0.62; –1.05	2.51	2.43

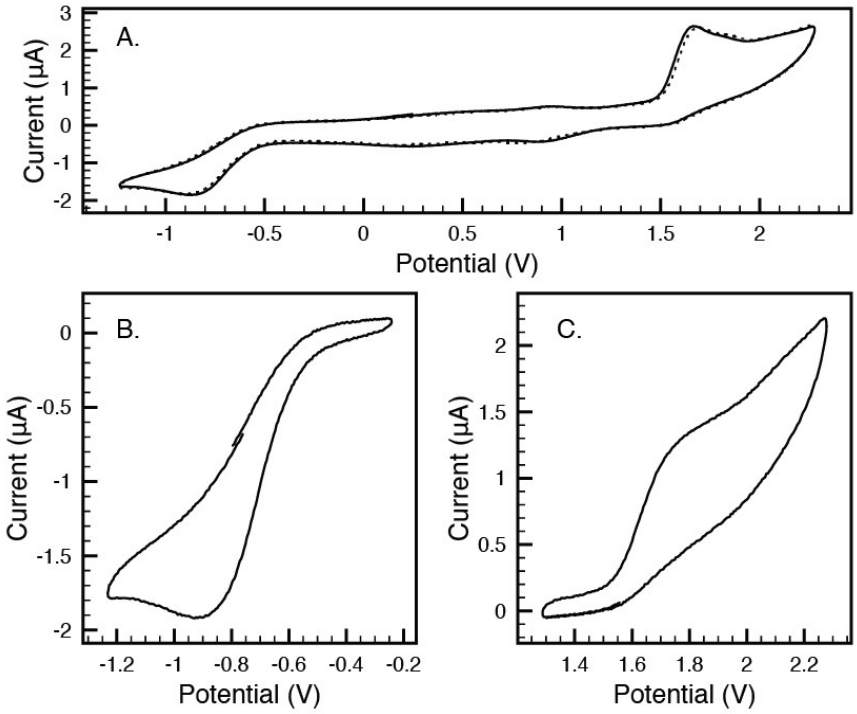

Figure S43. Cyclic voltammetry of [Cu(POP)(tzS)][BF_4] (**13**) in 0.1 M $NBu_4PF_6CH_3CN$ solutions using a platinum working electrode vs. NHE at 293 K.

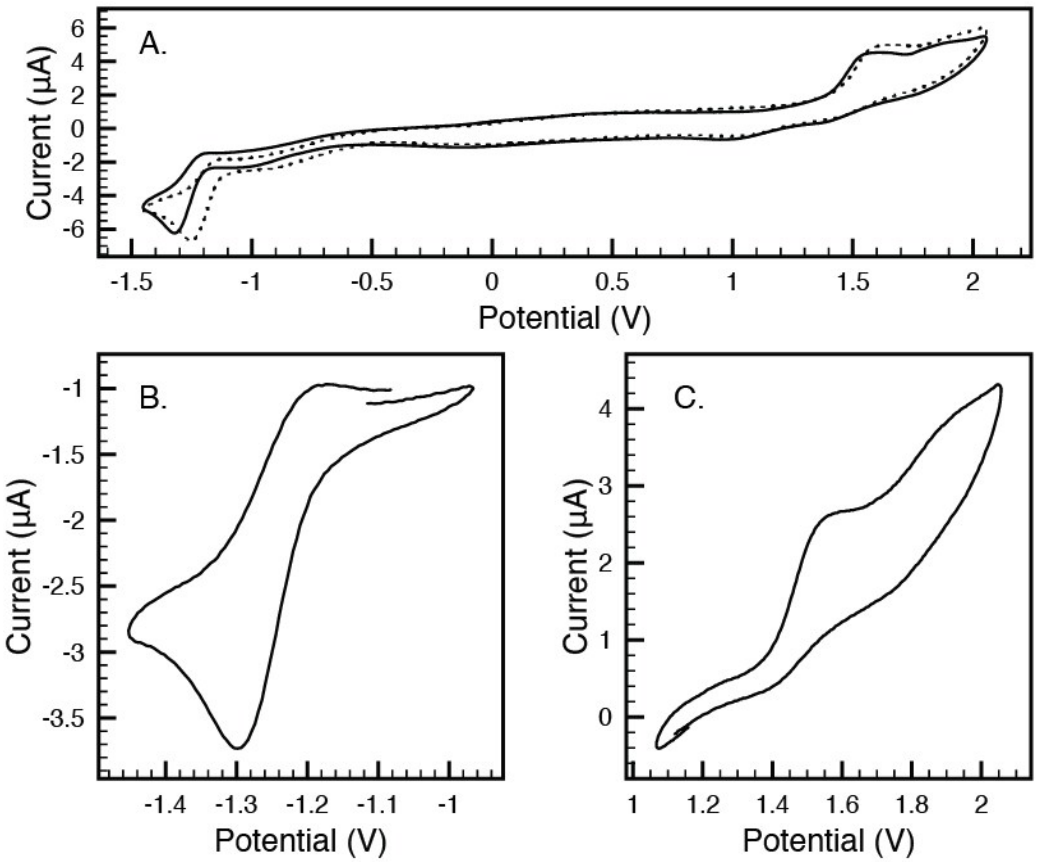

Figure S44. Cyclic voltammetry of [Cu(POP)($tzSO_2$)][BF_4] (**14**) in 0.1 M NH_4PF_6 CH_3CN solutions using platinum working electrode vs. NHE at 293 K.

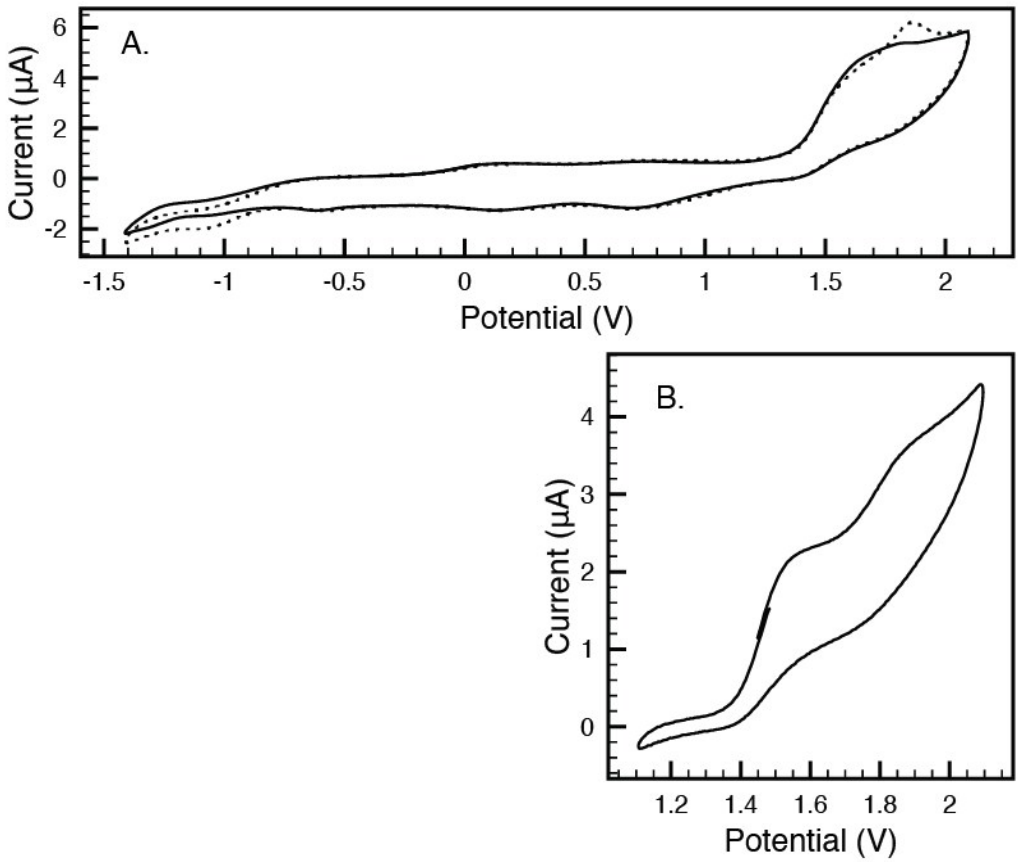

Figure S45. Cyclic voltammetry of [Cu(POP)(hbtz)][BF_4] (**15**) in 0.1 M NBu_4PF_6 CH_3CN solutions using platinum working electrode vs. NHE at 293 K.

REFERENCES

1 G. M. Sheldrick, *Acta Crystallogr. C*, 2015, **71**, 3–8.

2 O. V. Dolomanov, L. J. Bourhis, R. J. Gildea, J. A. K. Howard and H. Puschmann, *J. Appl. Crystallogr.*, 2009, **42**, 339–341.

3 A. L. Spek, *Acta Crystallogr. C*, 2015, **71**, 9–18.

4 K. Kalyanasundaram, *Coord. Chem. Rev.*, 1982, **46**, 159–244.

5 A. Begum and P. G. Pickup, *Electrochem. Comm.*, 2007, **9**, 2525–2528.